~~Glacial-interglacial contrasts in the marine inorganic carbon chemistry of the Benguela Upwelling System~~Contrasts in the marine inorganic carbon chemistry of the Benguela Upwelling System since the Last Glacial Maximum

Szabina Karancz[1]; Lennart J. de Nooijer[1]; Bas van der Wagt[1]; Marcel T. J. van der Meer[2], Sambuddha Misra[3]; Rick Hennekam[1]; Zeynep Erdem[2]; Julie Lattaud[4]; Negar Haghipour[5,6]; Stefan Schouten[2,7]; Gert-Jan Reichart[1,7]

[1] Department of Ocean Systems, NIOZ Royal Netherlands Institute for Sea Research, Texel, The Netherlands

[2] Department of Marine Microbiology and Biogeochemistry, NIOZ Royal Netherlands Institute for Sea Research, Texel, The Netherlands

[3] Centre for Earth Sciences, Indian Institute of Science, Bangalore, India

[4] Department of Environmental Sciences, University of Basel, Basel, Switzerland

[5] Geological Institute, Department of Earth Sciences, ETH Zürich, Zürich, Switzerland

[6] Laboratory of Ion Beam Physics, ETH Zürich, Zürich, Switzerland

[7] Department of Earth Sciences, Faculty of Geosciences, Utrecht University, Utrecht, The Netherlands

Correspondence to: Szabina Karancz (szabina.karancz@nioz.nl)

Abstract. Upwelling regions are dynamic systems where relatively cold, nutrient- and CO_2-rich waters reach to the surface from the deep. CO_2 sink or source properties of these regions are dependent not only on the dissolved inorganic carbon content of the upwelled waters, but also on the efficiency of the biological carbon pump that provides constraint on the drawdown of pCO_2 in the surface waters. The Benguela Upwelling System (BUS) is a major upwelling region with one of the most productive marine ecosystems today. However, contrasting signals reported on the variation in upwelling intensities based on, for instance, foraminiferal and radiolarian indices from this region over the last glacial cycle indicate that a complete understanding of (local) changes is currently lacking. To reconstruct changes in the CO_2 history of the Northern Benguela upwelling region over the last 27 ka BP, we used a box core (64PE450-BC6) and piston core (64PE450-PC8) from the Walvis Ridge. Here, we apply various temperature and pCO_2-proxies, representing both surface ($U^{K'}_{37}$, $\delta^{13}C$ of alkenones) and ~~intermediate depth~~subsurface (Mg/Ca, ~~B/Ca, S/Mg,~~ $\delta^{11}B$ in planktonic foraminiferal shells) processes. Reconstructed pCO_2 records suggest enhanced storage of carbon at depth during the Llast Ggglacial Mmaximum. The offset between $\delta^{13}C$ of planktonic (high $\delta^{13}C$) and benthic foraminifera (low $\delta^{13}C$) suggests an evidence of a more efficient biological carbon pump, potentially fuelled by remote and local iron supply through aeolian transport and dissolution in the shelf regions, effectively preventing release of the stored glacial CO_2.

1 Introduction

Upwelling systems are crucial components in the global carbon cycle thanks to intense biogeochemical cycling and enhanced biological productivity (Turi et al., 2014). Upwelling zones return the cold, nutrient- and CO_2-rich waters from depth to the surface which is also reflected in regional changes in surface water inorganic carbon chemistry. The connection between the deep and surface ocean thereby provides a potential mechanism linking changes in ocean circulation and chemistry with the atmosphere. Still, the shoaling of the thermocline and nutricline in these regions also favours phytoplankton growth to such a degree that these areas represent majority of the most productive regions of the ocean (Fig. 1 a). Thus, the leakage of CO_2 from the depths to the atmosphere is negated by biological sequestration, simultaneously rendering its quantification a challenging undertaking. The surface waters of the upwelling system undergo an increase in the partial pressure of CO_2 (pCO_2) and decrease in pH due to upwelling of deep CO_2-rich water. In turn, the enhanced primary productivity due to increased nutrients result in drawdown of pCO_2 by converting CO_2 into organic carbon, after which it may be returned to the deep ocean via the biological carbon pump (BCP; Volk and Hoffert, 1985; Longhurst and Glen Harrison, 1989; Ducklow et al., 2001; Turi et al., 2014; Hales et al., 2005; Muller-Karger et al., 2005). Ultimately, the net CO_2 flux from the ocean to the atmosphere is a function of the balance between upwelling strength (increase in CO_2) and efficiency of the BCP (drawdown of CO_2). On geological time scales this efficiency may have varied, potentially modulating ~~glacial-interglacial cycling of~~local air-sea CO_2 balance (Kohfeld et al., 2005; Kwon et al., 2009; Parekh et al., 2006; Hain et al., 2014).

The efficiency of the BCP determines how much of newly produced particulate organic carbon at the surface is transported to the deep (Volk and Hoffert, 1985; Hain et al., 2014). During primary production, nutrients are consumed (e.g., nitrate, phosphate; Redfield, 1958) from the surface ocean and dissolved inorganic carbon (DIC) is taken up in organic matter, which is also reflected by the enrichment in ^{13}C of the surface DIC (Degens et al.,

1968). This implies that we can use seawater carbon isotopes as proxy for the efficiency of the BCP. Seawater carbon isotopes can be reconstructed using the carbon isotopic composition ($\delta^{13}C$) in shells of carbonate producers, such as foraminifera. During high productivity periods the enhanced carbon uptake at the sea surface will enrich the shells of planktonic foraminifera in ^{13}C. At the same time, the ^{13}C-depleted carbon transported to the deep as organic matter will decrease the ^{13}C content of the deep water DIC pool, resulting in low $\delta^{13}C$ values in the benthic foraminifera shells (Fig. 1 b). Therefore, the difference between planktonic and benthic $\delta^{13}C$ provides a measure for the efficiency of the BCP, where more divergent values indicate a more efficient BCP (Hilting et al., 2008).

Reconstruction of inorganic carbon chemistry can be used to constrain past changes in CO_2-flux between the ocean and atmosphere (Fig. 1 c). Reconstruction of the complete inorganic carbon system is based on at least two parameters of this system (pCO_2, $[CO_3^{2-}]$, $[HCO_3^-]$, pH, [DIC] and total alkalinity), as well as on the knowledge of temperature and salinity (Zeebe and Wolf-Gladrow, 2001). Commonly used tracers for constraining parameters of the marine inorganic carbon chemistry are based on both organic (e.g., $\delta^{13}C$ of alkenones; Pagani et al., 2002; Pagani, 2014; Popp et al., 1998; Laws et al., 1995) and inorganic (e.g., $\delta^{11}B$ of foraminifera shells; Hemming and Hanson, 1992; Palmer and Pearson, 2003; Foster and Rae, 2016) proxy signal carriers, although these proxies rarely agree completely for upwelling regions (Seki et al., 2010; Palmer et al., 2010) or in general (Rae et al., 2021).

Here, we compare organic and inorganic proxies for temperature ($U^{K'}_{37}$, Mg/Ca) and the carbon system (alkenone-$\delta^{13}C$, foraminiferal-$\delta^{11}B$) with reconstructed efficiency of the BCP in the Benguela upwelling area to unravel the potential role of such areas in the known changes in atmospheric pCO_2 on glacial-interglacial time scales. Proxies for seawater carbon chemistry have specific inherent complications and their application require critical assumptions.

For instance, p~~P~~revious studies have observed discrepancy between alkenone based pCO_2 reconstruction and ice core records (Palmer et al., 2010; Andersen et al., 1999; Zhang et al., 2013; Witkowski et al., 2020; Jasper et al., 1994), which could be related to disequilibrium between sea surface and the atmosphere, especially at dynamic sites like upwelling regions. However, it may also be explained by the ~~mechanism~~process of CO_2 uptake in the algal cell, if passive diffusion is not the only way alkenone producers acquire CO_2 in the cell, as suggested by the traditional framework of this proxy (Bidigare et al., 1997)~~;~~. Alkenone-producers do use a carbon concentrating mechanism (CCM; Stoll et al., 2019; Reinfelder, 2011; Bolton and Stoll, 2013; Badger, 2021), which enables carbon acquisition in the cell through the active pumping of HCO_3^- to the chloroplast during low pCO_2 conditions. Also, pCO_2 reconstructions based on alkenone $\delta^{13}C$ values are subject to uncertainties related to the so-called *b* factor, that expresses the effect of multiple parameters related to the physiology of the alkenone producers (Jasper et al., 1994; Rau et al., 1996; Popp et al., 1998). Application of the *b* factor for the reconstruction of pCO_2 is much debated (e.g., Wilkes and Pearson, 2019) and an adaptation of CCM by the alkenone producers inevitably hampers the application of the proxy. However, there are examples of alkenone-based pCO_2 reconstructions reliably reproducing glacial-interglacial pCO_2 variability (Palmer et al., 2010; Jasper and Hayes, 1990; Bae et al., 2015), potentially related to specific local conditions. As the *b* value is best represented by a linear relationship to nutrient

Field Code Changed

Formatted: Font: Italic

Formatted: Subscript

Formatted: Font: Italic

Formatted: Subscript

Formatted: Font: Italic

Formatted: Subscript

Formatted: Font: Italic

availability (Bidigare et al., 1997). we here rely on the analysis of barium over calcium ratio (Ba/Ca) in planktonic foraminiferal shells that correlates with seawater Ba concentration, and hence is used as a proxy for seawater [PO_4^{3-}] (Lea and Boyle, 1989; Lea and Boyle, 1990b, a; Hönisch et al., 2011). ~~Therefore, we here also explore the recently suggested S/Mg ratio as a proxy for [CO_3^{2-}] as an additional constraint for past seawater carbon chemistry.~~

~~We~~ This study focuses on the Benguela Upwelling System (BUS) as it is one of the major upwelling regions, where strength of the upwelling and productivity changed over glacial/interglacial timescales. Whether upwelling intensity was stronger during glacial periods (Oberhänsli, 1991; Little et al., 1997; Kirst et al., 1999; Mollenhauer et al., 2003) or interglacial periods (Diester-Haass et al., 1992; Des Combes and Abelmann, 2007) is, however, still debated. Inconsistencies in the published body of work is possibly caused by seasonal differences between proxy signal carriers and/or major spatial (depth) related gradients, which is especially true for regions with strong CO_2 flux dynamics. Exchange of CO_2 between seawater and atmosphere at these regions may be constrained only by applying multiple proxies that comprise various living depth and seasonal preference. This at the same time allows comparing proxies and investigate (in)consistencies between different carbon system- and temperature proxies.

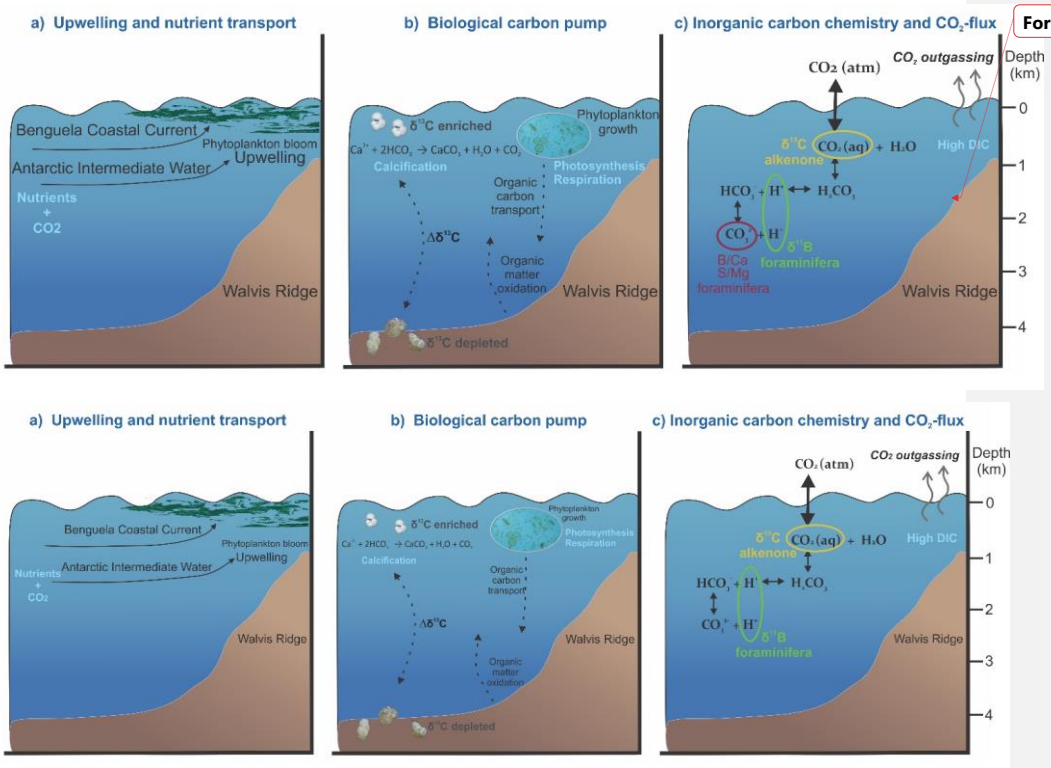

a) Upwelling and nutrient transport
b) Biological carbon pump
c) Inorganic carbon chemistry and CO2-flux

1

Formatted: Subscript
Formatted: Superscript
Formatted: Indent: Left: -1 cm

Figure 1: Cross sections of the Benguela Upwelling System depicting the characteristics of an upwelling region, where a) nutrient- and CO_2-rich waters are upwelled to the surface, b) high productivity contributes to the drawdown of CO_2 in the surface layers via the biological carbon pump, and c) the upwelling strength and efficiency of the biological carbon determines variations in the marine inorganic carbon chemistry, and hence CO_2-flux.

2 Oceanographic setting

The BUS is one of the four major Eastern Boundary Upwelling Systems, it is located between 15° and 34° S along the coastline of Africa (Hill, 1998; Hart and Currie, 1960). This region bears the highest productivity today among the Eastern Boundary Upwelling Systems, fuelled by nutrients transported mainly from the higher latitudes. Advection of the cold and nutrient rich water is a persistent phenomenon throughout the year (Carr, 2001; Chavez and Messié, 2009) and the magnitude of the particulate organic carbon (POC) flux from the surface to the deep exceeds 20 gC m^{-2} yr^{-1} (Henson et al., 2011; Laws et al., 2000; Devries and Weber, 2017).

The BUS is associated with the South Atlantic anticyclonic gyre which gives rise to upwelling on its' southeastern flank where it meets the African continent (Peterson and Stramma, 1991). The low-pressure system over western South Africa causes a pressure gradient between the continent and the ocean and thereby strengthen the southerly wind stress off the coast of Angola and Namibia. The interplay between the equatorward trade winds, the Coriolis-force, and the presence of the continental boundary lead to the offshore transport of surface waters. As such, this causes coastal upwelling of nutrient-rich South Atlantic Central Water (formed in the western South Atlantic; Stramma and England, 1999) and Antarctic Intermediate Water (AAIW). The upwelled waters are transported equatorward along the coast of Africa via the Benguela Current (BC) giving rise to high biological productivity. Filaments of high productive waters can be seen extending from the African continent (Fig. 2). Finally, the Walvis Ridge potentially plays a role in affecting local hydrography and hence the position of the upwelling (Peterson and Stramma, 1991).

The BC with its two main branches, the Benguela Oceanic Current and the Benguela Coastal Current, is the major northward flowing component of the BUS which joins the poleward flowing Angola Current in the north (Stramma and England, 1999). This convergence zone is located between 15°S and 18°S and is known as the Angola-Benguela frontal zone. The upwelling zone is bounded by warm current systems, the Angola Current system in the north and the Agulhas Current system in the south (Shannon and Nelson, 1996; Shillington, 1998; Shannon and O'toole, 2003). Hence, the BC is composed of a mixture of waters originated not only from the mid-latitude surface waters of the Central Southern Atlantic Ocean and the Southern Ocean but also from the Indian Ocean (Gordon, 1986; Lutjeharms and Valentine, 1987). This creates a north-to-south decrease in surface water temperature and salinity in the region (Santana-Casiano et al., 2009). Hydrographic changes in the region over glacial cycles have been related to changes in the transfer of Indian Ocean waters through Agulhas leakage variability (Knorr and Lohmann, 2003; Peeters et al., 2004; Scussolini and Peeters, 2013).

The BUS region is characterized by year-round upwelling but intensity varies over time due to the seasonal shift of the South Atlantic gyre. This results in stronger upwelling intensities in June-August compared to the rest of the year (Santana-Casiano et al., 2009; Kämpf and Chapman, 2016). The spatial and temporal dynamics of the BUS result in large variability in the associated CO_2 flux. Predominantly, it acts as a CO_2 source (Laruelle et al., 2014; Brady et al., 2019; Roobaert et al., 2019), but this may be interrupted by periods during which it acts as a CO_2 sink due to the high primary productivity (Gruber et al., 2009; Gregor and Monteiro, 2013).

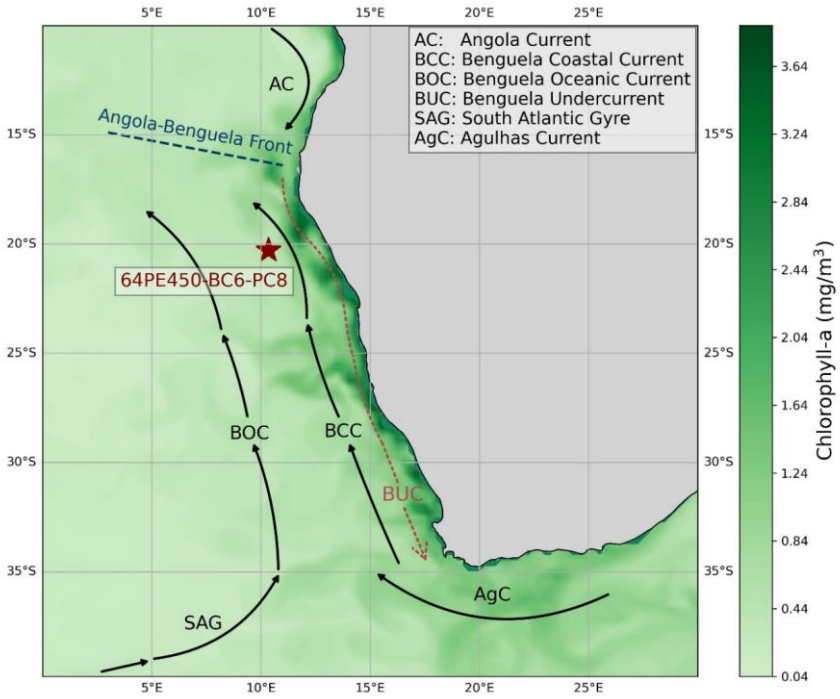

Figure 2: Map showing the location of sediment core 64PE450-BC6-PC8 and the dominant currents shaping the characteristics of the Benguela Upwelling System. The map is overlain with the distribution of surface water chlorophyll-a concentration of July 2023 obtained from Global Ocean Biogeochemistry Analysis and Forecast (E.U. Copernicus Marine Service Information; https://doi.org/10.48670/moi-00015). High chlorophyll-a concentrations indicate the high productivity and nutrient-rich upwelled waters of this region today.

3 Materials and methods

Samples were taken from box core 64PE450-BC6 and piston core 64PE450-PC8 retrieved from the south flank of the Walvis Ridge, both taken at the same location (approximately -20.29 S, 10.35 E) at a water depth of ~1375 mbss. The box core consisted of 40.5941.5 cm of sediment, whereas the piston core collected 1453 cm (cut into

15 sections, of which we ~~used~~ dated the first 100 cm ~~within this study~~). The top of the piston core was missing and, hence, we ~~combined both the~~used the BC ~~and~~ to supplement the missing top of the PC ~~to~~ and obtain a near continuous record ~~with a composite depth of 141.5 cm~~, which we here refer to as 64PE450-BC6-PC8. The composite record was sampled with a resolution varying between 2 and 5 cm to optimize coverage of the glacial-interglacial transition. All samples were freeze-dried and subsequently split in sub-samples to obtain lipid biomarkers and foraminifera from the same core depth.

3.1 Foraminiferal sample cleaning

Due to their high abundance in upwelling regions as well as common use in paleoclimate reconstructions (e.g., Spero and Lea, 1996), we here selected specimens of *Globigerina bulloides* for the planktonic foraminifera-based records. Freeze-dried samples were washed over a 63 µm sieve, dried and further dry sieved to separate size fractions 150-315 µm and 315-425 µm. Specimens of *G. bulloides* were picked from the latter size fraction for analysis of oxygen and carbon isotopes, minimizing any potential impacts of ontogeny. However, as much more specimens were needed, the smaller size fraction was used for radiocarbon, element / calcium (El/Ca), and boron isotope analysis. The foraminifer's size has been shown to affect boron isotopes of several planktonic foraminifera species (Hönisch and Hemming, 2004; Henehan et al., 2013; Henehan et al., 2016), and hence size fraction need to be minimized to avoid inducing uncertainties related to ontogenetic variability. The species investigated within those studies (*T. sacculifer*, *G. ruber*, *O. universa*) are all symbiont-bearing planktonic foraminifera that are affected by pH change in their microenvironments due to the symbionts' physiological processes (i.e., respiration, photosynthesis). The degree of pH alteration is dependent on symbiont abundance/density, which is proportional to foraminiferal shell size. To avoid such impact on shell $\delta^{11}B$, we here used *G. bulloides*, which is a symbiont-barren species. To construct a benthic foraminiferal carbon isotope record, specimens of *Cibicidoides wuellerstorfi* were picked from the 315-425 µm size fraction.

Formatted: Font: Italic
Formatted: Font: Italic
Formatted: Font: Italic
Formatted: Superscript
Formatted: Font: Italic

Foraminiferal samples were cleaned prior to the analysis of El/Ca ratios and stable isotopes, following an adapted protocol of Barker et al. (2003). This adapted protocol is as follows: for the analysis of the shells' element concentrations in solution and the boron isotopic composition, specimens were carefully cracked using a scalpel to open up the chambers and release potential clay content from the inside. The samples were subsequently transferred to acid cleaned 1.5 mL vials (Treff) and rinsed three times with deionized water (Milli-Q), twice with methanol, followed by another thorough rinse with deionized water, using ultra-sonification for each rinsing step. To remove all organic material from the shells, samples were placed in a hot block and oxidized with NH_4OH-buffered 1% H_2O_2 solution for 45 minutes at 90 °C. To ensure complete removal or organic material, this step was repeated up to three times based on visual inspection. After the oxidative cleaning, the samples were transferred to new pre-cleaned vials (Treff) and leached with diluted acid (1 mM HNO_3) followed by rinsing the samples three times with deionized water. Because the boron isotope analysis is very sensitive to contamination two additional leaching steps with 1% NH_4OH were added followed by rinsing with deionized water before the acid leaching. Samples for El/Ca and $\delta^{11}B$ analysis were finally dissolved in 500 µL 0.1 M ultra grade HNO_3 and in 75-80 µL 0.5 M ultra grade HNO_3, respectively.

Specimens taken for the analysis of El/Ca ratios with LA-Q-ICP-MS and for the measurement of $\delta^{18}O$ and $\delta^{13}C$ were cleaned following the same clay removal and oxidative cleaning step as described above but without cracking the shells before the cleaning steps.

3.2 Radiocarbon analysis

Radiocarbon analysis ($^{14}C/^{12}C$) on 50-100 specimens of well-preserved shells of *G. bulloides* were performed at Laboratory of Ion Beam Physics, ETH Zürich. The analysis of $^{14}C/^{12}C$ followed the protocol described in Wacker et al. (2013; 2014). Briefly, samples were measured with a gas ion source in a Mini Carbon Dating System (MICADAS; Synal et al., 2007) with an automated method for acid digestion of carbonates (Wacker et al., 2013). Samples were placed in 4.5 mL exetainers vials (Labco Limited®, UK) and purged with a flow of 60 mL min^{-1} of helium for 10 minutes and subsequently leached with 100 µL 0.02 M ultrapure HCl with an automated syringe to remove adsorbed contaminants. Analysis of the released CO_2 from both the leachate and remaining sample provided confirmation for the near complete removal of contaminants. The released CO_2 from the leachate was directly transported by helium to a zeolite trap and injected into the ion source for $^{14}C/^{12}C$ analysis. The remaining leached sample was acidified with 100 µL ultrapure H_3PO_4 (85%) and heated at 60 °C for a minimum of 1 hour. The released CO_2 was then injected in the ion source for analysis (Wacker et al., 2014; Fahrni et al., 2013). The difference between the radiocarbon values of the leachate and leached samples were less than 5%. Radiocarbon determinations are given in the conventional radiocarbon ages and corrected for isotopic fractionation via $^{13}C/^{12}C$ isotope ratios. Calibration was performed using the Marine20 calibration curve (Heaton et al., 2020) with a local correction to the marine reservoir age (ΔR) of 146 ± 85 ^{14}C years (Dewar et al., 2012). These calculations were computed using the Bayesian age-depth model in the Bacon v2.3 package for the R statistical programming software (Blaauw and Christen, 2011).

3.3 Analysis of stable oxygen and carbon isotopes

Pre-weighed 20-40 µg of the shells of *G. bulloides* were dissolved in orthophosphoric acid and analysed at 71 °C by a Kiel IV device coupled to a MAT 253 Isotope Ratio Mass Spectrometer (IRMS, Thermo Fischer Scientific®) at the NIOZ. Analyses were calibrated using standard bracketing (NBS-19) and the NIOZ house standard (NFHS-1; Mezger et al., 2016) was used to monitor drift. Accuracy and precision for $\delta^{13}C$ = 1.922 ± 0.05 ‰ and $\delta^{18}O$ = -2.189 ± 0.11 ‰ were calculated across several analytical runs (± 1σ SD, n = 47).

3.4 Analysis of foraminiferal Element/Calcium ratios

Prior to the analysis of the samples in solution, a few planktonic foraminifera specimens were screened for preservation to minimize the possibility of diagenetic overprint affecting the geochemical signature of the shells. For this, the ratios of $^{23}Na/^{43}Ca$, $^{24}Mg/^{43}Ca$, $^{25}Mg/^{43}Ca$, $^{27}Al/^{43}Ca$, $^{55}Mn/^{43}Ca$ $^{88}Sr/^{43}Ca$ were simultaneously monitored during the ablation of single chambers of *G. bulloides* by Laser Ablation Quadrupole Inductively Coupled Plasma Mass Spectrometer (LA-Q-ICP-MS). Laser ablation data was acquired on 60-µm diameter spots with a repetition rate of 4 Hz and a laser energy density of ~1 J cm^{-2}. The JCp (*Porites sp.* coral) nano-pellet was used to monitor instrumental drift and JCt (*Tridacna gigas* giant clam; Okai et al., 2004), MACS-3 and the NIOZ Foraminifera House Standard-2-Nano-Pellet (NFHS-2-NP; Boer et al., 2022) provided further quality control on

the measurement. NIST SRM610 was used as calibration standard. Data was evaluated both as profiles and shell averages.

Approximately 40-50 specimens of *G. bulloides* were dissolved for solution analyses using a Sector-Field Inductively Coupled Plasma Mass Spectrometer (SF-ICP-MS, Thermo Fischer Scientific® Element-2). Applied cleaning procedure is based on Barker et al. (2003) as discussed above. A pre-scan of calcium concentrations ($[Ca^{2+}]$) was performed on an aliquot of 30 µL of the dissolved samples and based on that data subsequently all samples were diluted to match $[Ca^{2+}]$ (100 ppm) for element analyses. Isotopes of ~~^{11}B,~~ ^{25}Mg, ^{138}Ba were measured in low resolution ~~and ^{32}S in medium resolution to avoid interference~~. All samples were measured against 4 ratio calibration standards (De Villiers et al., 2002) and alternated with 0.1 M HNO_3 in between samples to increase the efficiency of wash-out. All samples are drift-corrected using the NFHS-1 standard (Mezger et al., 2016) and three additional standards: NFHS-2 (Boer et al., 2022), JCp, and JCt (Okai et al., 2004), to evaluate accuracy and precision of the analytical runs. Uncertainty from the internal precision on the basis of short term stability is < 2 % for both ~~B,~~ Mg, and Ba~~, and S~~. Samples were analysed in replicates yielding an uncertainty of ~~< 3.25 µmol mol^{-1} for B,~~ < 0.02 mmol mol^{-1} for Mg, ~~and S,~~ and < 0.14 µmol mol^{-1} for Ba.

3.5 Micro-distillation and boron isotope analysis

Approximately 150 specimens of *G. bulloides* were cleaned for the analysis of boron isotopes. Boron was separated from the calcium carbonate matrix via the micro-distillation technique (Gaillardet et al., 2001; Wang et al., 2010; Misra et al., 2014). 70 µL of the sample was placed on the lid of a Teflon® fin-legged conical beaker (5 mL) and placed upside down on a hotplate at 100 °C for 20-24 hours. The fin-legged vials were wrapped in aluminium foil to provide a heat gradient for a more efficient separation of boron. Once the micro-distillation was complete, the vials were carefully removed from the hotplate while turning them over and subsequently left for cooling. Sample residue was removed with putting new lids on the beakers and each sample was diluted with 0.2 M HF + 0.2 M HNO_3 for a pre-scan of the boron concentration ([B]). Based on the results of the pre-scan, a final dilution was made to set [B] at 5 ppb for the analysis of $\delta^{11}B$.

Analysis of the micro-distilled samples was performed at the NIOZ on a Neptune Plus Multi-Collector Inductively Coupled Mass Spectrometer (MC-ICP-MS, Thermo Fisher Scientific®) equipped with high performance extraction cones (Jet sample cone and 'X' skimmer cone) to maximize sensitivity for boron. Samples were injected using a Savillex® 50 µL min^{-1} C-flow nebulizer and Teflon® Scott type spray chamber. Beams of ^{10}B and ^{11}B were measured on L3 and H3 Faraday cups equipped with amplifiers using $10^{13}\Omega$ resistors (Misra et al., 2014; Lloyd et al., 2018). The instrument was tuned to obtain a stable sensitivity, typically 15-25 mV ppb^{-1} B.

Solutions of 0.2 M HF + 0.2 M HNO_3 were used for rinsing throughout the analytical run between analyses, and as matrix for each sample and standard. The analysis followed the approach of sample-standard bracketing using NIST 951 as reference standard. All samples and quality control standards were analysed in duplicates and thus here average values with ± 2σ standard deviations are reported. Samples with a replicate precision higher than ± 0.6 ‰ (2σ) were excluded from this study. A coral standard (Chanakya and Misra, 2022) was treated with the complete carbonate cleaning and micro-distillation procedure for each analytical sequence and repeatedly

analysed to monitor long term precision ($\delta^{11}B$ = 24.57 ± 0.65 ‰ 2σ, n = 64). Additionally, non-micro-distilled AE-121 standard was analysed within each run for quality control ($\delta^{11}B$ = 19.48 ± 0.33 ‰ 2σ, n = 46).

In addition to the coral standard, the initial test analysis to validate the boron purification method and instrumental accuracy and precision also included repeated measurements of seawater (Southern Ocean, $\delta^{11}B$ = 39.72 ± 0.25 ‰ 2σ, n = 5) and a boron standard (AE-121) mixed with $CaCO_3$ (trace metal basis, Acros Organics®) to mimic foraminiferal calcium concentrations ($\delta^{11}B$ = 19.53 ± 0.25 ‰ 2σ, n = 18).

3.6 Estimating past salinity and foraminifera-based temperatures, pH, and pCO_2

Sea surface temperatures (SST) were calculated from foraminiferal Mg/Ca values using the species specific temperature calibration of Mashiotta et al. (1999),

$$Mg/Ca = 0.47\ (\pm 0.03)^{0.107(\pm 0.003)*SST}, \quad (1)$$

where propagated error was calculated based on 1 standard deviation of the duplicate analysis of Mg/Ca and the uncertainty derived from the calibration equation. Mg/Ca values of planktonic foraminifera are known to be affected by salinity changes as well (Gray et al., 2018; Dueñas-Bohórquez et al., 2009), however, a correction for this effect requires an independent estimate for salinity and a species-specific calibration. The same is true for the effect of pH (Gray et al., 2018; Gray and Evans, 2019). Moreover, as both effects are relatively minor and adding them would also introduce additional uncertainties, we here decided to refrain from correcting for salinity and/or pH when calculating past temperatures.

For calculating past carbon~~ate~~ chemistry, salinity is an important parameter and it was estimated based on its conservative relationship with relative sea level change (Waelbroeck et al., 2002). Modern seawater salinity of the BUS (35.43 ± 0.30) was derived from the WOCE Global Data Version 3.0 (Schlitzer, 2000) based on the five closest datapoints to the location of core 64PE450-BC6-PC8.

The measured $\delta^{11}B$ values of *G. bulloides* were converted into pH (Hemming and Hanson, 1992) using Eq. (2):

$$pH = pK_B - \log(-(\delta^{11}B_{sw} - \delta^{11}B_{borate}) / (\delta^{11}B_{sw} - \alpha * \delta^{11}B_{borate} - \varepsilon)), \quad (2)$$

where the equilibrium constant, pK_B (Dickson, 1990), was calculated for each sample based on SST derived from the Mg/Ca values of *G. bulloides* and salinity based on sea level. The fractionation factor between $B(OH)_3$ and $B(OH)_4^-$, expressed here as α, is 1.0272 ± 0.0006, from which fractionation, ε, is derived as 27.2 ± 0.6 (Klochko et al., 2006). Boron isotopic composition of seawater, $\delta^{11}B_{sw}$ is 39.61 ± 0.2 ‰, based on a large range of temperature, salinity and depth conditions (Foster et al., 2010), and the $\delta^{11}B$ of borate was calculated from the measured $\delta^{11}B$ of *G. bulloides* using the species~~–~~specific core-top calibration from Raitzsch et al. (2018).

Uncertainty on the reconstructed pH value was determined for each sample through error propagation that considered the above described uncertainties of pK_B, α, ε, $\delta^{11}B_{sw}$ and the standard deviation (external uncertainty) based on duplicate or triplicate analysis of foraminiferal $\delta^{11}B$.

Concentrations of CO_2 are based on pH and inorganic carbon chemistry calculations using the PyCO2SYS package (Humphreys et al., 2022) in Python version 3.11.2. Uncertainty is propagated for each computed carbon chemistry parameter as described in Humphreys et al. (2022).

3.7 Lipid extraction and alkenone analyses

Lipids were extracted from the freeze-dried and homogenized sediment samples using an accelerated solvent extractor (ASE® 350, DIONEX®) at the NIOZ. Samples were extracted with dichloromethane (DCM) and methanol (9:1, *v/v*) at 100 °C to obtain the total lipid content and subsequently dried under N_2 gas at 35 °C in a Caliper TurboVap LV Evaporator. Samples were then redissolved in DCM and run through an Na_2SO_4 column to eliminate excess water. The extract was passed through an alumina (Al_2O_3) column and separated into apolar, ketone and polar fractions using a mixture of hexane : DCM (9:1, *v/v*), hexane : DCM (1:1, *v/v*), and DCM : methanol (1:1, *v/v*), respectively. All extracts were dried under N_2 and the ketone fraction was further utilized to obtain the relative abundance and $\delta^{13}C$ values of the long chain alkenones.

Ketone fractions were dissolved in ethyl acetate and concentrations of alkenones were measured using a gas chromatograph with flame ionization detection (GC-FID, Agilent® 6890N) equipped with silica capillary column (CP-Sil 5 CB; 50 m x 0.32 mm, 0.12 µm film thickness). The temperature program of the GC-FID analyses used an initial temperature of 70 °C that increased with a rate of 20 °C min^{-1} to 200 °C followed instantly by heating at a rate of 3 °C min^{-1} until it reached 320 °C where it remained constant for 10 minutes.

Based on the initial concentration measurement, samples were diluted with ethyl acetate to allow stable carbon isotope analysis using a gas-chromatography-isotope ratio-mass spectrometer (GC-IRMS, Thermo Fisher Scientific® Delta V Advantage Trace® 1310). The GC-IRMS was equipped with crossbond trifluoropropylmethyl polysiloxane columns (Rtx-200; 60m x 0.32, 0.5 µm film thickness) and helium as a carrier gas. Each sample was manually injected on the GC-IRMS. The starting temperature of the GC-IRMS was 70 °C which then increased with 18 °C min^{-1} until reaching 250 °C. After reaching that temperature heating continued with 1.5 °C min^{-1} until 320 °C, where it was kept stable for 25 minutes. Samples were analyzed for carbon isotopes in duplicates and instrumental accuracy was monitored through measurement of the of B5 *n*-alkane mixture standard (provided by A. Schimmelmann, Indiana University) every day (i.e. after every 6-7 samples). The isolink II combustion reactor was oxidized for 10 minutes every day before the start of standard and sample analysis. Each analysis was followed by 2 minutes of seed oxidation to maintain the reactor oxygenated.

3.8 Calculation of alkenone based temperatures and pCO_2

Alkenone-based sea surface temperatures were derived from ketone unsaturation index ($U^{K'}_{37}$), where $U^{K'}_{37}$ is defined as the relative abundance of di- and tri-unsaturated C_{37} methyl alkenones (Prahl and Wakeham, 1987):

$$U^{K'}_{37} = C_{37:2} / (C_{37:3} + C_{37:2}). \quad (3)$$

Sea surface temperature was then calculated using the alkenone temperature calibration model developed for the Atlantic region (Conte et al., 2006).

Fractionation of stable carbon isotopes during photosynthesis ($\varepsilon_{p37:2}$) can be computed based on the difference between the carbon isotopic ratio of aqueous carbon dioxide ($\delta^{13}C_{CO2}$) and the organic biomass ($\delta^{13}C_{org}$):

$$\varepsilon_{p37:2} = [(\delta^{13}C_{CO2} + 1000) / (\delta^{13}C_{org} + 1000) - 1] \times 1000. \quad (4)$$

$\delta^{13}C_{CO2}$ was derived from the carbon isotopes of planktonic foraminifera, *G. bulloides* ($\delta^{13}C_p$) corrected for the temperature dependent fractionation during calcite precipitation (Romanek et al., 1992) and the fractionation between dissolved and gaseous carbon dioxide (Mook et al., 1974).

$\delta^{13}C_{org}$ was calculated from the carbon isotopes of di-unsaturated alkenones ($\delta^{13}C_{37:2}$) as

$$\delta^{13}C_{org} = [(\delta^{13}C_{37:2} + 1000) * / (1 - \Delta\delta^{13}C_{org} + 1)] - 1000, \quad (5)$$

where $\Delta\delta^{13}C_{org}$ expresses the carbon isotopic difference between $C_{37:2}$ and DIC, that has been defined between 3 – 6 ‰ based on culture experiment (Riebesell et al., 2000; Schouten et al., 1998; Van Dongen et al., 2002). We here take the commonly applied value of 4.2 ‰ (Bijl et al., 2010; Pagani et al., 2005; Pagani et al., 2010; Pagani et al., 2011; Seki et al., 2010; Palmer et al., 2010).

Based on $\varepsilon_{p37:2}$, aqueous CO_2 ($[CO_2]_{aq}$) can be reconstructed as followed (Hayes, 1993; Pagani et al., 2002):

$$[CO_2]_{aq} = b / (\varepsilon_f - \varepsilon_{p37:2}), \quad (6)$$

where ε_f stands for the carbon isotopic fractionation associated with carbon fixation estimated as 25 ‰ (e.g., Popp et al., 1998). Parameter *b* expresses all physiological factors affecting total carbon isotope fractionation that includes cell shape and size, membrane permeability as well as the algae's growth rate (Jasper et al., 1994; Rau et al., 1996; Popp et al., 1998; Conte et al., 1994; Riebesell et al., 2000). Earlier studies using phytane (Bice et al., 2006; Damsté et al., 2008) and alkenone (Witkowski et al., 2018) to reconstruct pCO_2 estimated *b* for a mean value of 165 - 170 ‰ kg μM^{-1}. As growth rate and thereby nutrient availability have a large influence on the physiological factors and, accordingly, *b* values are highly correlated to $[PO_4^{3-}]$ (Bidigare et al., 1997), *b* can be best described at our core site by estimating past changes in $[PO_4^{3-}]$ (Pagani et al., 2005). Here, $[PO_4^{3-}]$ is estimated based on the ~~barium over calcium ratio (~~Ba/Ca~~)~~ ratio of planktonic foraminifera, *G. bulloides* (Lea and Boyle, 1989; Lea and Boyle, 1990b, a; Martin and Lea, 1998; Lea and Boyle, 1991). We therefore constrain past changes in b as (Pagani et al., 2005):

$$b = [118.52 \times (Ba/Ca \times [PO_4^{3-}]_{modern} / Ba/Ca_{modern}) + 81.4284.07]. \quad (7)$$

Average modern PO_4^{3-} concentration ($[PO_4^{3-}]_{modern}$) in the BUS is 0.63 µmol kg^{-1} (obtained from GLODAPv2023; Lauvset et al., 2024; Olsen et al., 2016; Key et al., 2015) whereas the corresponding modern foraminiferal Ba/Ca value (Ba/Ca_{modern}) was analyzed here (19.08 µmol mol^{-1}). Eq. (7) basically assumes a constant and proportional relation between Ba and $[PO_4^{3-}]$. This seems reasonable for our purposes as surface water Ba concentration has been shown to be reflected proportionally in foraminiferal Ba/Ca (Lea and Boyle, 1991; Hönisch et al., 2011) and the cold nutrient rich surface waters are generally enriched in dissolved barium (e.g., Davis et al., 2020).

To calculate atmospheric pCO_2 from aqueous concentrations of CO_2, Henry's law was applied using the temperature and salinity dependent solubility constant, K_0.

$$pCO_2 = [CO_2]_{aq} / K_0. \quad (8)$$

Uncertainty propagation for the calculated pCO_2 values was based on the errors derived from 1 standard deviation of duplicate analysis of $\delta^{13}C$ of the extracted ketone fraction, $\delta^{13}C$ of foraminifera and Ba/Ca values of foraminifera. The largest uncertainty in alkenone based pCO_2 reconstructions originates from the estimated past $[PO_4^{3-}]$ and to incorporate potential variation in nutrient levels during the deglaciation, an additional uncertainty of 0.2 µmol kg^{-1} was assigned to the known modern values of $[PO_4^{3-}]$. This uncertainty is based on the gradient measured today in upper 50 meters of the water column, which is more than the variability observed in surface water today, but also includes potential changes in the upwelled waters.

4 Results

4.1 Radiocarbon ages

The calibrated mean radiocarbon ages generally increase with depth in both BC and PC cores used here. Sediment core 64PE450-BC6 comprises ~~41.5~~40.59 cm, where the core-top sample was dated at 4.863 ~~± 0.284~~ ka BP, and an age of 9.551 ~~± 0.248~~ ka BP at 40 cm bsf (Fig. 3 a). This suggests an average sedimentation rate of about 0.01 cm yr^{-1}, with somewhat higher values (> 0.01 cm yr^{-1}) at the top 12 cm. ~~,~~ Radiocarbon dates at the top of the box core (0-11 cm) indicate reversed ages (4.9 ka at 11 cm and 5.2 ka at 1 cm uncalibrated ages). This interval also corresponds to elevated Ca/Al, Ti/Al, and Si/Al ratios measured through X-Ray Fluorescence (XRF)-core-scanning (Supplementary Fig. S1; Weltje and Tjallingii, 2008). The enrichment of elements commonly found in coarse fractions and heavy minerals is likely due to the removal of fine fraction material by winnowing, which may have also contributed to the loss of the last 4.8 ka BP in the sedimentary record. Alternatively, the upper 10 cm bsf have constant ages due to bioturbation. Radiocarbon analyses from sediment core 64PE450-PC8 included 6 samples of the upper 100 cm of sediment collected. The age-depth model for this core suggests 9.994 ~~± 2.042~~ ka BP years at 5 cm bsf depth (Fig. 3 b) and indicates the presence of a disturbed core-top. ~~, which is likely due to the loss of sediment at the top (common during piston coring).~~ Low sedimentation rates (0.002 cm yr^{-1}) characterize the top 10 cm bsf of this core which is approximately in line with the sedimentation rate at the deepest parts of box core 64PE450-BC6 (~0.006 cm yr^{-1}). However, average sedimentation rate in 64PE450-PC8 is lower (0.004 cm yr^{-1}) compared to the average values observed in the box core, which, in part, might also be due to compaction with increasing depth. The top 60 cm bsf of the core shows a steady increase in sedimentation rate (0.002 – 0.007 cm yr^{-1}) and therefore the low average values may be attributed to a relatively abrupt decrease in sedimentation rate at 60 cm bsf in the core, which correspond to an age of 23.586 ~~± 0.410~~ ka BP. Between 60 and 100 cm bsf depth sedimentation rates remain 0.001 – 0.002 cm yr^{-1}.

To align the box core and the piston core, lightness reflectance data (l*) was used here as an additional constraint to the radiocarbon dates (Supplementary Fig. S2). The detailed reflectance data (63 µm resolution) shows an overlap between the two cores. The top 4.24 cm of 64PE450-PC8 (i.e., the disturbed core-top) overlaps with approximately 30.14 cm of 64PE450-BC6 (i.e., from 10.45 to 40.59 cm bsf). This suggests severe compression

Formatted: English (United Kingdom)

Formatted: English (United Kingdom)

of the top of 64PE450-PC8, likely due to the piston coring, but the overlap can still be used to align the age model of the two cores. Due to the uncertainty related to sediment deposition ~~at these depths and the low sedimentation rate~~between 60 and 100 cm bsf of the piston core, further analysis of this study focuses only on the ~~41.5~~40.59 cm bsf of the core 64PE450-BC6 and upper 65.5 cm bsf of core 64PE450-PC8, which together comprise a near-continuous time interval from ~5 to 27 ka BP .

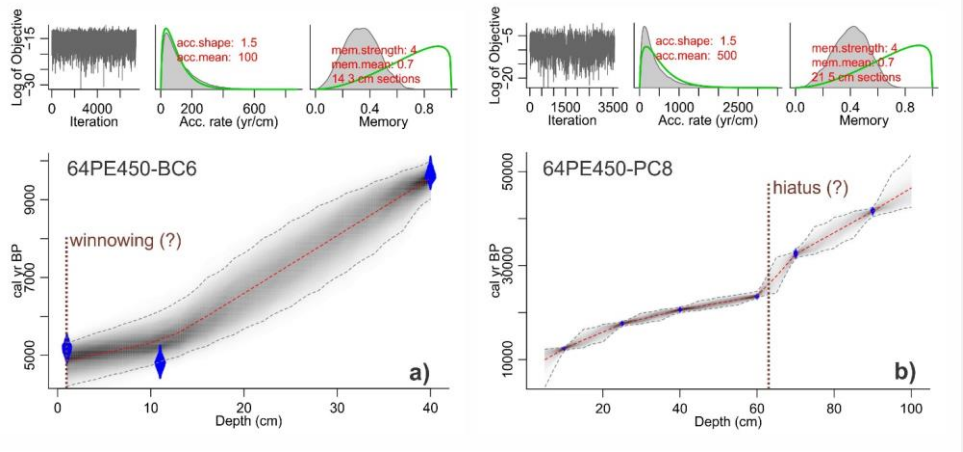

Figure 3: Age-depth model of a) 64PE450-BC6 (box core) and b) 64PE450-PC8 (piston core) based on radiocarbon dates, where blue diamonds indicate the sampling depth for ^{14}C analysis. The calibration of radiocarbon ages and the figure was generated using the Bacon v2.3 package for the R statistical programming software (Blaauw and Christen, 2011). Calibration was performed using the Marine20 calibration curve (Heaton et al., 2020) with a local carbon reservoir correction (ΔR) of 146 ± 85 ^{14}C years (Dewar et al., 2012). Red dashed lines show mean values of the best fitted model and grey dashed lines indicate 95% confidence interval. Note, that ~~both panel a) and b) show the complete sediment records acquired by the box corer and piston corer, respectively, but~~ due to the disturbed core-top and potential hiatus in the piston core as indicated in panel b), only ~~the top~~the interval from 4.25 to 65.5 cm of 64PE450-PC8 was ~~utilized~~ used for temperature and carbon system reconstruction in this study.

4.2 Stable isotopes

Carbon isotope values of the planktonic foraminifer, *G. bulloides*, vary between -1.4 ‰ and 0.6 ‰ (VPDB). The glacial part of the record is marked by relatively high $\delta^{13}C$ values with a maximum of 0.6 ‰ at 23.3 ka BP. After that, there is a rapid decrease to a minimum value of -1.1 ‰ at 22 ka BP, then it stabilizes around -0.8 ‰ until 18 ka BP (Fig. 4 a). The $\delta^{13}C$ values of the benthic foraminifer, *C. wuellerstorfi*, although measured at somewhat lower resolution, range between 0.5 ‰ and 1.0 ‰. It appears that there is a continuous increase in benthic $\delta^{13}C$ from 27 ka BP until the most recent sample (Fig. 4 a).

The $\delta^{18}O$ values of *G. bulloides* range from 0.0 ‰ (VPDB) to 3.2 ‰ with the most depleted values at ~8 ka BP (Fig. 4 b). During the glacial, $\delta^{18}O$ values decreased from the highest values at 23.6 ka BP (peak glacial), showing rapid changes during the deglaciation, subsequently decreasing again gradually before reaching a plateau at about

10 ka BP. During the Holocene these values stayed relatively stable and varied only between 0.0 ‰ and 0.6 ‰ (VPDB). The trend differs from the lower resolution benthic record of $\delta^{18}O$ measured on *C. wuellerstorfi* (Fig. 4 b). The benthic foraminiferal $\delta^{18}O$ values are consistently higher compared to the *G. bulloides* values, which is in line with lower bottom water temperatures. This difference, however, appears smaller during the end glacial than during the Holocene.

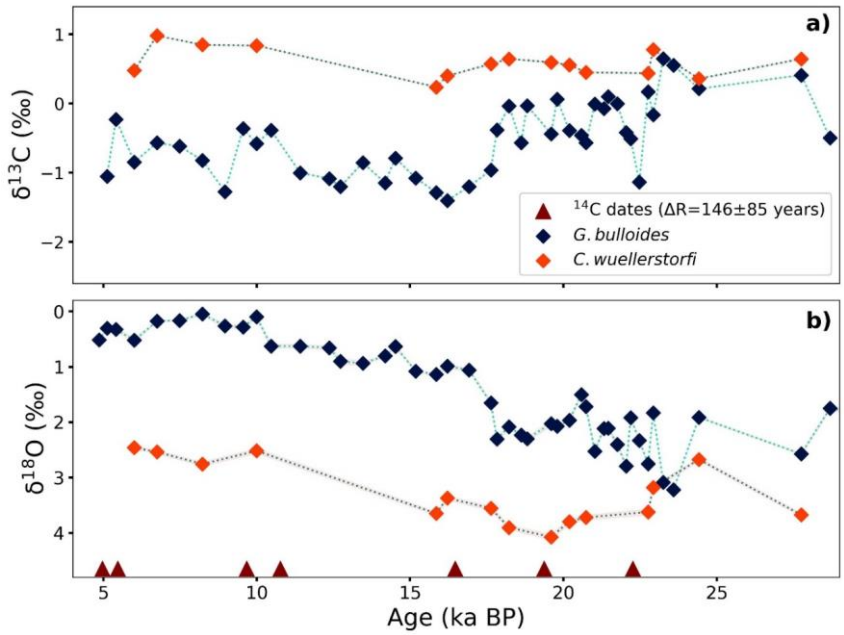

Figure 4: a) $\delta^{13}C$ and b) $\delta^{18}O$ values of planktonic (*G. bulloides*) and benthic (*C. wuellerstorfi*) foraminifera plotted with the age model. Red triangles indicate the ages tied with radiocarbon dates.

The boron isotopic composition of the planktonic foraminifer, *G. bulloides*, ranges between 15.1 and 17.0 ‰ (relative to NIST 951) with larger variations during the last 6-5 ka BP (Fig. 5 a). The lowest $\delta^{11}B$ values were observed at 5.4 ka BP, whereas $\delta^{11}B$ values reach a maximum at 13.5 ka BP. Prior to this maximum value, $\delta^{11}B$ values show an increasing trend from 27.8 to 13.5 ka BP (Fig. 5 a).

The carbon isotopic composition of the alkenones shows its heaviest value (-22.4 ‰) at 19.6 ka BP. After this peak, $\delta^{13}C$ values reach a minimum (-23.4 ‰) at 15.9 ka, then increasing again towards the most recent values (-22.7 to -22.9 ‰; Fig. 5 b).

4.3 Element/Ca ratios in the planktonic foraminifer, *G. bulloides*

Mg/Ca reaches maximum values of 2.85 and 2.81 mmol mol^{-1} at 16.9 and 6.7 ka BP, respectively (Fig. 5 c). Substantially lower values characterise the interval between 16.9 and 6.7 ka BP, when Mg/Ca ranges between

2.46 and 2.69 mmol mol^{-1}. The lowest values (2.30-2.40 mmol mol^{-1}) were found at 4.9-5.4 ka BP and 21.3-27.8 ka BP.

The general trend in foraminiferal Ba/Ca shows an increase from glacial to recent (Fig. 5 d). ~~The general trend in foraminiferal B/Ca values shows an increase from glacial to recent (Fig. 5 c). The highest B/Ca value (52 µmol mol^{-1}) is observed in the top of the record and the lowest value (35 µmol mol^{-1}) at 22.8 ka BP. Somewhat higher variability is observed between 22.8 and 15.2 ka BP, with B/Ca values ranging between 35 and 48 µmol mol^{-1}.~~

~~S/Ca values show a trend opposite to that observed for B/Ca. While S/Ca shows a maximum (1.33 mmol mol^{-1}) at 18.6 ka BP, it decreases to 0.93 mmol mol^{-1} at 5.1 ka (Fig. 5 d). Overall the record shows a gradual change in foraminiferal S/Ca, without much scatter.~~

The oldest part of the record shows relatively stable Ba/Ca values at around 6 µmol mol^{-1}. During the last 15 ka BP, however, more variability is observed for Ba/Ca ~~(Fig. 5 e)~~. ~~The here observed trends are not resembling the trends observed for either B/Ca or S/Ca. However, the overall increasing trend from 27 ka BP to present day Ba/Ca values somewhat coincides with the trend in B/Ca.~~The highest Ba/Ca value (19.1 µmol mol^{-1}) is observed in the top of the record and the lowest values, 4.02 and 3.94 µmol mol^{-1} at 17.6 and 27.8 ka BP, respectively.

~~Mg/Ca reaches maximum values of 2.85 and 2.81 mmol mol^{-1} at 16.9 and 6.7 ka BP, respectively (Fig. 5 f). Substantially lower values characterise the interval between 16.9 and 6.7 ka BP, when Mg/Ca ranges between 2.46 and 2.69 mmol mol^{-1}. The lowest values (2.30-2.40 mmol mol^{-1}) were found at 4.9-5.4 ka BP and 21.3-27.8 ka BP.~~

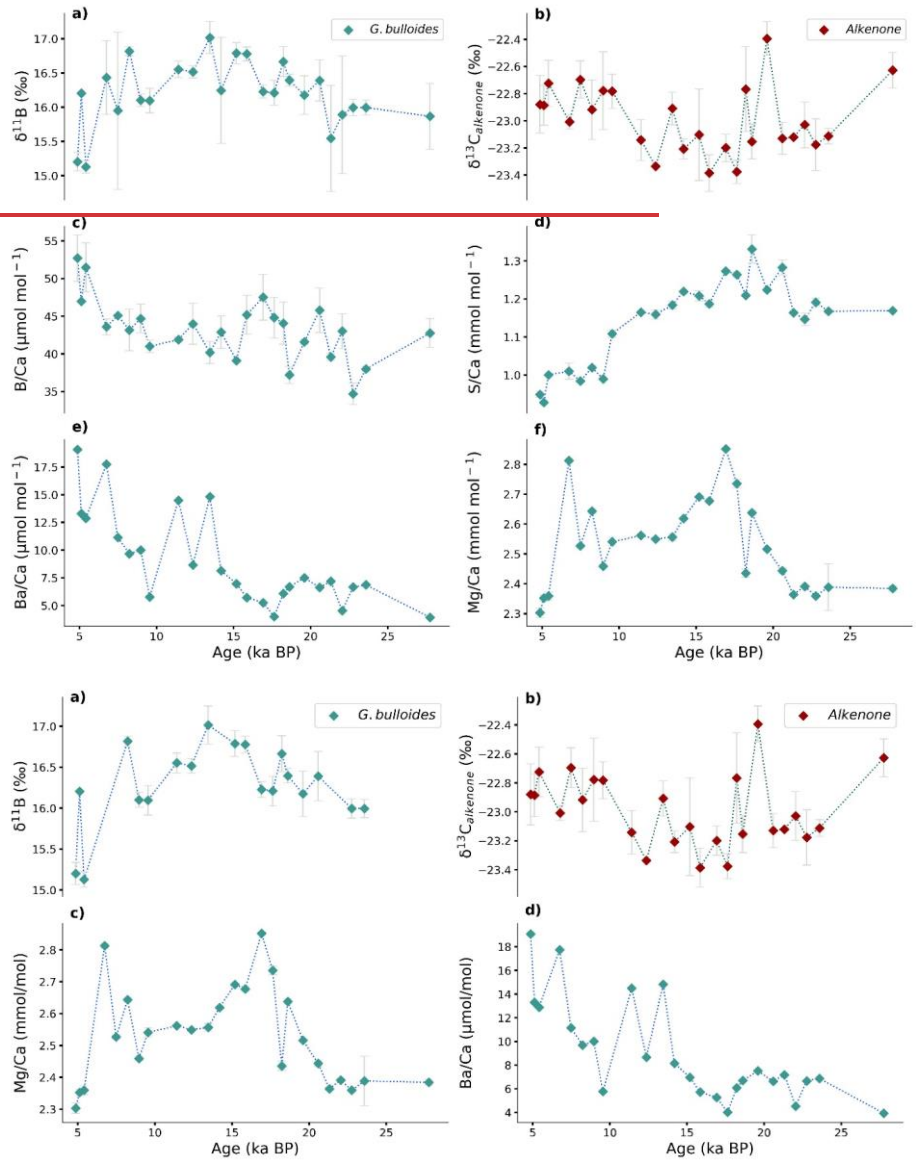

Figure 5: Measured a) foraminiferal $\delta^{11}B$, b) alkenone $\delta^{13}C$, and foraminiferal element concentrations: c) Mg/Ca, B/Ca, d) S/Ca, e) Ba/Ca, f) Mg/Ca plotted over the past 27 ka BP at the Benguela Upwelling System. Error bars show ± 1σ standard deviation. When error bars are is not shown, the error of the duplicate measurement is smaller than the symbol.

4.4 $U^{K'}_{37}$ sea surface temperatures

The alkenone based $U^{K'}_{37}$ record shows continues increase throughout the deglaciation (Supplementary Fig. S~~1~~3). The lowest value (0.56) was measured at 27 ka BP which increases to 0.58 until 26.3 ka BP. The interval of 22.0 - 19.6 ka BP records again low $U^{K'}_{37}$ values, which then follows a steady increase until 9.6 ka BP. During the early Holocene $U^{K'}_{37}$ values stabilize around 0.7 until 6.8 ka BP when values slightly start to decrease reaching 0.67 in the uppermost part of the record.

5 Discussion

5.1 Local temperatures over the LGM, last deglaciation, and Holocene

The proxy-based temperature reconstructions ~~indicate most of the well-known~~resemble to the Southern Hemisphere climate responses based on the gradual temperature increase from 23 ka BP onwards (e.g., Petit et al., 1999; Suggate and Almond, 2005; Clark et al., 2009). However, comparing these reconstructions with both Northern (NGRIP; North Greenland Ice Core Project Members, 2004) and Southern Hemisphere ~~events, such as found within the δ^{18}O ice core record from EPICA-Dome C~~ (EPICA-Dome C; EDC; Jouzel et al., 2007) records, it is evident that individual climate events show similarities also to the trends observed in the Northern Hemisphere (Fig. 6). This suggests that the location of 64PE450-BC6-PC8 was affected by both Northern and Southern Hemisphere climatic changes. ~~for the last 27 ka BP (Fig. 6).~~

The $U^{K'}_{37}$ based sea surface temperature reconstruction shows low temperatures (18.2 – 18.5 °C) between 23.6 and 18.6 ka BP (Fig. 6 a) ~~corresponding to~~indicating the last glacial maximum (LGM; e.g., Clark et al., 2009; Hughes et al., 2013) within this record. Oxygen isotopes from the shells of *G. bulloides* show more enriched values during the same period and hence indicate low sea surface temperatures, in agreement with $U^{K'}_{37}$, however, with significantly more scatter in δ^{18}O values (1.5 – 3.2 ‰). Foraminiferal δ^{18}O values not only depend on temperature, but also on the stable oxygen isotopic signature of the water and hence salinity. Meltwater is transported to large distances with the AAIW, that will result in larger regional impact in the upwelling zone than in the global ocean. Therefore, shifts in e.g. sea ice extension or river runoff, might also have impacted local seawater δ^{18}O and hence foraminiferal oxygen isotopes. Similarly, multiple studies suggested an overall reduced Agulhas leakage during the LGM compared to deglacial levels (Pether, 1994; Flores et al., 1999; Rau et al., 2002; Peeters et al., 2004; Charles and Morley, 1988; Wefer et al., 1996; Franzese et al., 2006), and changes therein could also have resulted in enhanced δ^{18}O variability during the LGM.

Our record shows a rapid warming following the onset of deglaciation from ~17.8 ka BP observed in both the alkenone~~-~~based SST reconstruction and δ^{18}O values of *G. bulloides* (Fig. 6 d). The last glacial termination (approximately 18 ka BP) resulted in the extensive release of meltwater on the Northern Hemisphere, weakening Atlantic Meridional Overturning Circulation (AMOC; Mcmanus et al., 2004; Rahmstorf, 2002; Denton et al., 2010; Hodell et al., 2017; Pöppelmeier et al., 2023). This, in turn changed global heat distribution and hence the cooling in the North Atlantic region known as the Heinrich Stadial 1~~1~~ (e.g., Bond et al., 1993; Cacho et al., 1999;

Mcmanus et al., 1994), which was accompanied by a warming in the Southern Hemisphere (e.g., Calvo et al., 2007; Wang et al., 2013).

Following ~~the Heinrich Stadial I~~the rapid warming, further, more gradual temperature increase during the deglaciation is evident from the $U^{K'}_{37}$ temperatures, while only a slight decrease in $\delta^{18}O$ values is observed between 14.6 and 13.0 ka BP. ~~T~~During the same~~h~~ time interval the ~~e~~ Antarctic Cold Reversal (ACR) during the Bølling-Allerød Northern Hemisphere warming (e.g., Pedro et al., 2016; Blunier et al., 1997) is known to cause~~, resulted in~~ either no change (Lamy et al., 2007) or a slight decrease in SST (Vandergoes et al., 2008). ~~Moreover, here~~Here, the data resolution does not allow assigning trends in temperature change to this event, and we observed only minor changes between the trends in alkenone (increasing trend) and the foraminiferal Mg/Ca based SST (decreasing trend; Fig. 6 b) and the $\delta^{18}O$ (decreasing trend) signal. Offsets likely reflect differences in either seasonality between coccolithophores and *G. bulloides* (Leduc et al., 2010), or differences in water depth where the signals were recorded. Hence, minor differences between the records could be due to a shift in productive season and or a shift in depth habitat. Because offsets are only minor (< 4.4 °C) unravelling these signals is highly speculative.

At approximately 12.7 ka BP, we see a slight increase in both $U^{K'}_{37}$ and $\delta^{18}O$ based temperatures, which is in line with the general Southern Hemisphere temperature record (Rühlemann et al., 1999; Kaplan et al., 2010; Panmei et al., 2017; Blunier and Brook, 2001). The Younger Dryas (Alley, 2000 and references therein) started around this time with another meltwater discharge into the North Atlantic, weakening overturning circulation, and leading to simultaneous warming in the Southern Hemisphere (Broecker, 1998; Stocker, 1998).

The most recent part of the record, the early Holocene, shows a cooling trend ~~following the 8.2 ka BP event known from the Northern Hemisphere~~. Although represented by only one datapoint in our record, the observed warming at around 8 ka BP (here and in Ljung et al., 2008) could be a local signal due ~~assigned~~ to the well-known cooling in the Northern Hemisphere in line with the AMOC slow down during this event (Barber et al., 1999; Matero et al., 2017).

The SST reconstruction based on foraminiferal Mg/Ca values is generally in line with the $U^{K'}_{37}$ and $\delta^{18}O$ record, confirming overall trends. Absolute values, however, differ, which is likely due to depth differences between the proxy signal carriers. Alkenone-based temperature reconstruction agrees with reported SSTs from the upper 50 m of the Northern Benguela (Santana-Casiano et al., 2009), while the foraminifer based temperature (Mg/Ca) corresponds to the values observed somewhat deeper (100-150 m, GLODAPv2023; Lauvset et al., 2024; Supplementary Fig. S4). Vertical dispersion of *G. bulloides* may be large, but this suggested living habitat corresponds well with previously reported living depths for this species (Tapia et al., 2022; Lessa et al., 2020; Rebotim et al., 2017). Whereas the LGM and the deglaciation are clearly visible in Mg/Ca, $U^{K'}_{37}$, and the $\delta^{18}O$ records, during the Holocene the Mg/Ca temperature record clearly deviates from the other two. The offset between $U^{K'}_{37}$ and foraminiferal Mg/Ca values during the LGM is about 3.0 °C, and this gradually increases to 5.6 °C during the early Holocene. This implies that foraminiferal Mg/Ca values are affected by other factors than SST alone. Partial dissolution of foraminiferal shells at depth may also affect Mg/Ca values and thereby reconstructed

temperatures through the preferential loss of Mg^{2+} (Dekens et al., 2002; Regenberg et al., 2006). However, impact of dissolution is probably minor only as the water depth at site 64PE450-PC8-BC6 is less than 1.4 km and *G. bulloides* is reported to be less sensitive to dissolution compared to other surface dwellers (Mekik et al., 2007). Whereas Mg/Ca values may also be affected by early diagenesis (Hover et al., 2001; Kozdon et al., 2013; Ni et al., 2020; Panieri et al., 2017; Sexton et al., 2006; Stainbank et al., 2020), El/Ca ratios in the shell's profile obtained through laser ablation did not show any evidence for such diagenetic effects.

Nevertheless, the trends observed in the different proxies seem to accurately represent the deglacial climate patterns, albeit that foraminiferal Mg/Ca based temperatures may be affected by some changes in depth habitat or seasonality of *G. bulloides*.

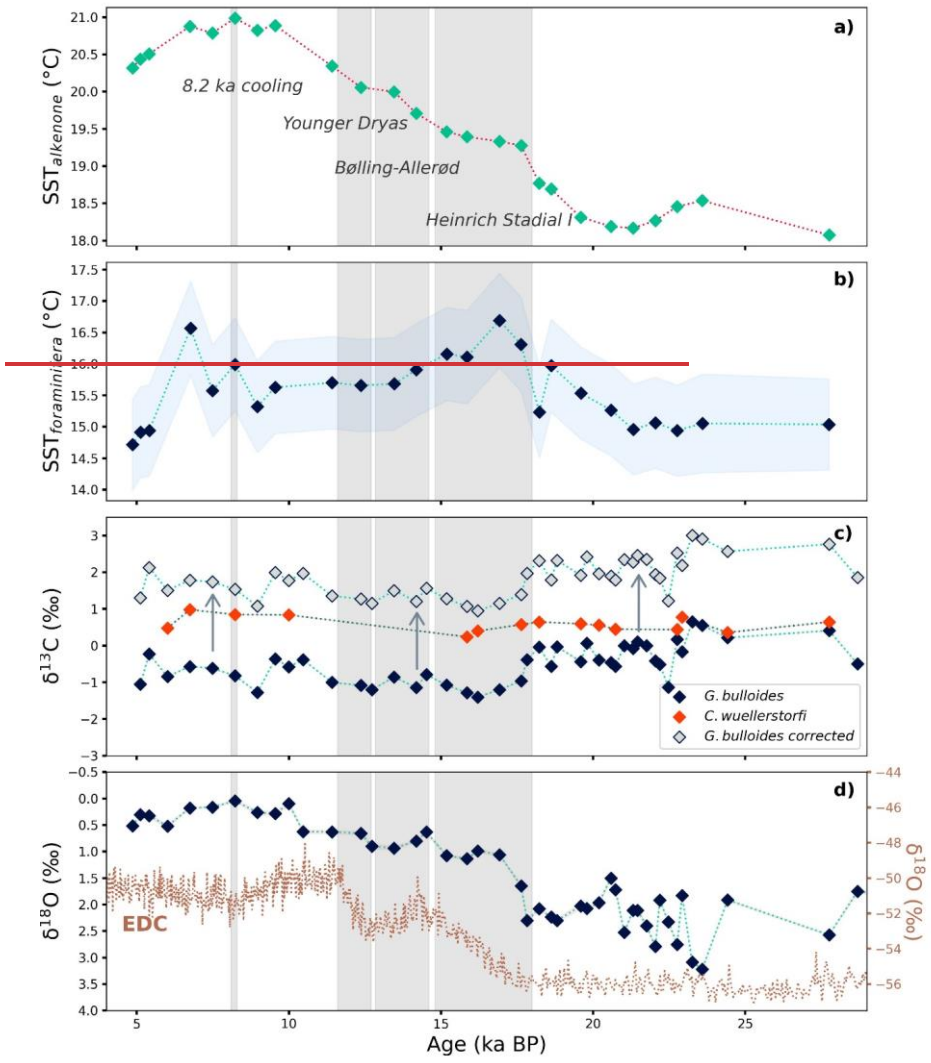
a)
b)
c)
d)
8.2 ka cooling
Younger Dryas
Bølling-Allerød
Heinrich Stadial I
SST alkenone (°C)
SST foraminifera (°C)
δ13C (‰)
δ18O (‰)
G. bulloides
C. wuellerstorfi
G. bulloides corrected
EDC
Age (ka BP)

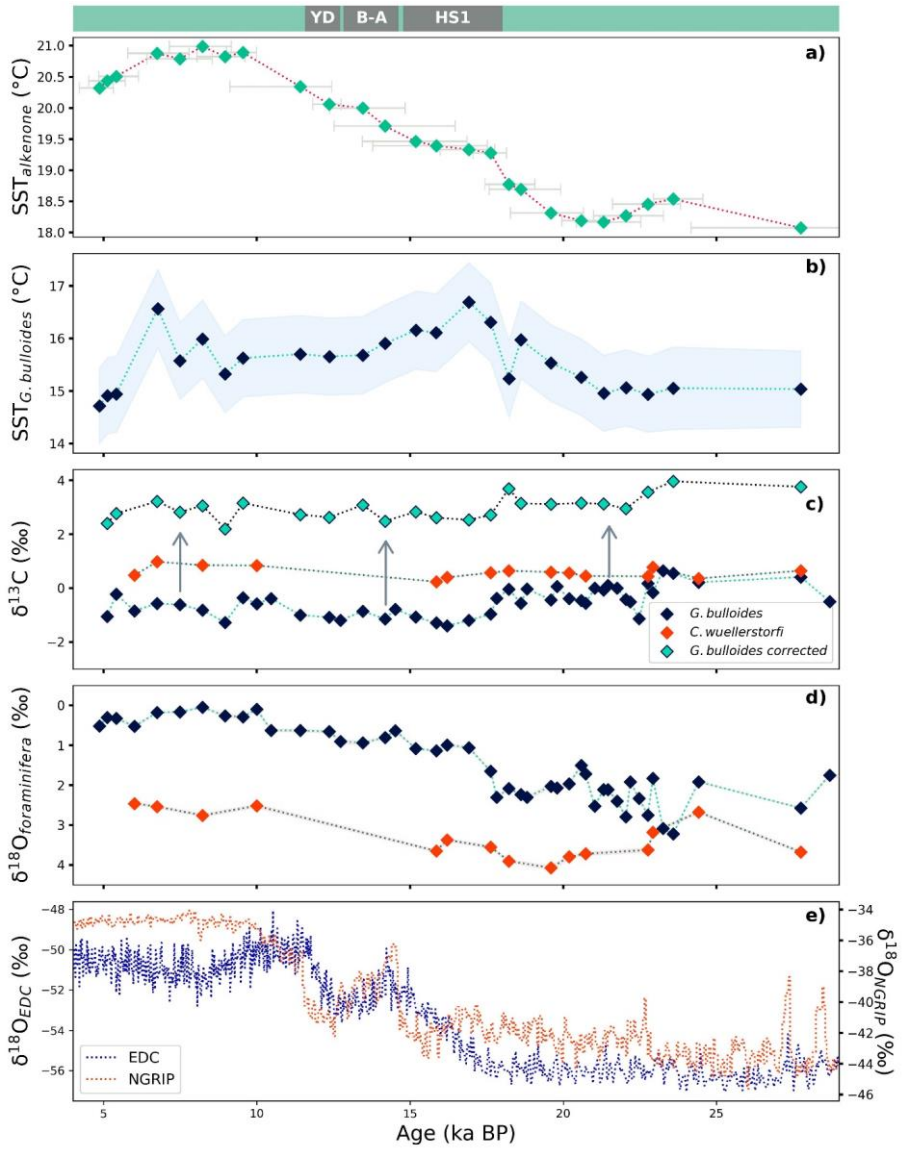

Figure 6: Reconstructed sea surface temperatures (SST) based on a) the alkenone unsaturation index, $U^{K'}_{37}$, and b) foraminiferal Mg/Ca, c) $\delta^{13}C$ analysed in benthic (*C. wuellerstorfi*) and planktonic (*G. bulloides*) foraminifera with corrected values, ~~and~~ d) $\delta^{18}O$ of benthic (*C. wuellerstorfi*) and planktonic (*G. bulloides*) foraminifera, and e) $\delta^{18}O$ ice core record from EPICA-Dome C (EDC; Jouzel et al., 2007) and North Greenland Ice Core Project (NGRIP; North Greenland Ice Core Project Members, 2004) shown for the past 27 ka BP. Corrected $\delta^{13}C$ values of *G. bulloides* marked with green diamonds in panel c) are based on temperature (derived from Mg/Ca ratios; Bemis et al., 2000) and $[CO_3^{2-}]$ values (derived from pH and TA; Bijma et al., 1999), and arrows indicate the direction of the correction. Modern day SST at core site

Formatted: Font: Italic

Formatted: Font: Not Italic

Formatted: Font: Italic

Formatted: Subscript

Formatted: Superscript

64PE450-BC6-PC8 is approximately 20.7 °C (GLODAPv2023; Lauvset et al., 2024; Santana-Casiano et al., 2009). ~~Grey shaded areas mark climate events as labelled on the uppermost panel. Blue shaded area in panel~~**Major climate events (YD: Younger Dryas; B-A: Bølling-Allerød interval; HS1: Heinrich Stadial 1) are marked above the top panel as reference. Horizontal error bars in panel a) show the age uncertainty based on 95 % confidence interval of the calibrated age. Blue shaded area in panel b) indicates the error propagated from temperature calibration uncertainty and ± 1σ standard deviation of the duplicate measurement of the samples. Analysis of the stable isotopes (panel c and d) provided an error smaller than the symbols shown on the figure.** ~~Arrows in panel c) indicate the direction of the correction on the planktonic foraminiferal $\delta^{13}C$.~~

Formatted: Dutch (Netherlands)

5.2 Biological carbon pump

Comparing benthic (*C. wuellerstorfi*) and planktonic (*G. bulloides*) trends in $\delta^{13}C$ shows they have similar values during the last glacial and higher $\delta^{13}C$ values for the benthic than for the planktonic foraminifera during the interglacial. This is in contrast to what one would expect if BCP determined the foraminiferal carbon isotope signatures (Hain et al., 2014; Hilting et al., 2008). Generally, DIC in surface waters is enriched in ^{13}C as the BCP results in preferential export of ^{12}C rich organic matter to the deeper water masses, where it is released through remineralization. The efficiency and strength of the BCP is known to be affected by multiple processes, such as the formation, sinking, and interaction of aggregates with other minerals (Fowler and Knauer, 1986; Alldredge and Silver, 1988; Armstrong et al., 2001; Francois et al., 2002; Klaas and Archer, 2002; De La Rocha and Passow, 2007; Turner, 2015), and the efficiency is generally reflected by the offset in ^{13}C between the surface and deep water ($\Delta\delta^{13}C$). However, species specific offsets from equilibrium values between seawater DIC $\delta^{13}C$ and foraminiferal carbonate $\delta^{13}C$ can challenge interpretation of the $\Delta\delta^{13}C$ and are likely responsible for the here observed lower $\delta^{13}C$ values of *G. bulloides* compared to *C. wuellerstorfi*.

Application of foraminiferal $\Delta\delta^{13}C$ as a proxy for BCP efficiency requires a direct relation with the $\delta^{13}C$ of DIC. Benthic foraminiferal $\delta^{13}C$ values, and in particular $\delta^{13}C$ values of the epifaunal *C. wuellerstorfi*, are generally considered faithful recorders of the $\delta^{13}C$ values of DIC, with carbonate $\delta^{13}C$ values being close to equilibrium (Thomas and Shackleton, 1996; Hilting et al., 2008). The stable carbon isotopic composition of DIC today is approximately 0.5 – 0.7 ‰ at a depth of 1.3 km along the latitude 20° S (Kroopnick, 1980; Kroopnick, 1985; Sarnthein et al., 1994; Curry and Oppo, 2005; Schmittner et al., 2013) which agrees well with the value inferred from *C. wuellerstorfi* in the uppermost sample (6.0 ka BP) of core 64PE450-BC6-PC8.

Stable carbon isotopic values from planktonic foraminifera have been shown to be generally lower with respect to the equilibrium values of DIC (Kahn, 1979; Kahn and Williams, 1981; Oppo and Fairbanks, 1989; Spero, 1992), indicating a strong biological impact (i.e. the vital effect; e.g., Spero, 1992; De Nooijer et al., 2014; Erez, 2003). For instance, symbiont-bearing species such as *O. universa* and *T. sacculifer* show offsets in $\delta^{13}C$ as much as 1.8 and 1.4 ‰ respectively, depending on irradiance level (Spero, 1992; Spero and Lea, 1993). Although *G. bulloides* lacks algal symbionts (Hemleben et al., 1989) it has been shown to deviate even more from the ambient seawater $\delta^{13}C$ values (Kahn and Williams, 1981; Spero and Lea, 1996). Several factors likely add together to the observed offset, such as carbon chemistry ($[CO_3^{2-}]$; 0.3-1.0 ‰; Spero et al., 1997; Bijma et al., 1999), temperature,

(2.4-2.6 ‰; Bemis et al., 2000) and respiration (Zeebe et al., 1999). More recently, Bird et al. (2017) suggested that also bacterial symbiosis may partly explain the observed offset for $\delta^{13}C$ in *G. bulloides*. While symbiont photosynthesis contributes to elevating foraminiferal $\delta^{13}C$ due to preferential ^{12}C removal, geochemical signature of *G. bulloides* is more likely to be controlled by the respiration of photoautotrophic cyanobacteria that produces depleted CO_2 and hence, decreases shell $\delta^{13}C$ values (Bird et al., 2017). Irrespective of the process involved, a substantial correction has to be applied to the $\delta^{13}C$ values of *G. bulloides* to approach the heavier seawater DIC $\delta^{13}C$ values. Increasing temperature (Bemis et al., 2000) and $[CO_3^{2-}]$ (Bijma et al., 1999) will also increase the offset between $\delta^{13}C$ values of *G. bulloides* and seawater [DIC] suggesting that larger corrections are required during the Holocene than during the last glacial. Still, when the corrections for changes in temperature and $[CO_3^{2-}]$ are applied, trends remain the same, showing the highest $\delta^{13}C$ values of planktonic foraminifera during the LGM (Supplementary Fig. S5~~3~~). Hence, despite the uncertainties in interpreting the absolute planktonic $\delta^{13}C$ values, the trend in $\Delta\delta^{13}C$ should still provide a measure for changes in the efficiency of the BCP. We here applied ~~a constant equilibrium offset of 2.4 %~~a combined correction for both temperature ~~(Fig. 6 c) which is the average correction required based on temperature variation in our record~~ (Bemis et al., 2000) and $[CO_3^{2-}]$ (Bijma et al., 1999), derived from foraminiferal Mg/Ca and $\delta^{11}B$, respectively (Fig. 6 c). ~~This~~ The ~~value is close to the~~ offset of the $\delta^{13}C$ value of the core-top sample with the modern $\delta^{13}C$ values of the DIC is approximately 2.4 ‰ (Kroopnick, 1985), which agrees with the applied corrections based on temperature and $[CO_3^{2-}]$ in the most recent samples (2.4 – 2.8 ‰; 4.9-5.4 ka BP). ~~.~~

Formatted: Subscript

Formatted: Superscript

Offsets between the $\delta^{13}C$ of the planktonic and benthic foraminifera reflect differences in the BCP, but potentially also changes in the dominant water mass at the cores' locations. Intermediate depths of the South Atlantic are dominated today by the Antarctic Intermediate Water and this likely remained the major water mass over the last glacial cycle (Pahnke et al., 2008; Howe et al., 2016; Gu et al., 2017). However, it is unclear whether the depth range of the AAIW increased (Muratli et al., 2010) or decreased (Ronge et al., 2015; Li et al., 2021) during the LGM compared to present day. In the western Atlantic, $\delta^{13}C$ values of benthic foraminifera suggest persistence of AAIW water masses at the depth of our core site (e.g., Curry and Oppo, 2005). As our values correspond to those found by Curry and Oppo (2005) we suggest also here a sustained influence of southern water masses, with the $\delta^{13}C$ value of DIC in the AAIW during the LGM remaining relatively similar to present day. ~~The analysed $\delta^{13}C$ values of benthic foraminifera from the LGM in this study show on average values that are 0.2 ‰ lower values than those during the Holocene.(Curry and Oppo, 2005)~~

Variations in the stable carbon isotopic composition of surface seawater DIC are attributed to the changes in biological activity and air-sea exchange (Lynch-Stieglitz et al., 1995). While enhanced biological activity will result in an increase of $\delta^{13}C$ values of DIC, more intense air-sea exchange will contribute to a decrease. In upwelling regions, the upwelled light carbon may still result in a net decrease in $\delta^{13}C$ values despite the enhanced biological activity. The analysed $\delta^{13}C$ values of benthic foraminifera from the LGM in this study show on average values that are 0.2 ‰ lower values than those during the Holocene. This glacial-interglacial difference is 0.1 ‰ higher than what was observed in the western South Atlantic (Curry and Oppo, 2005), which could be caused by a change in the $\delta^{13}C$ of the source waters during the glacial. Still, an offset of 0.1 ‰ due to the less efficient air-sea CO_2 exchange does not affect the final conclusions.

Summarizing the observed impacts, assuming a more or less stable presence of AAIW at intermediate depth and after correcting for offsets, a larger difference between planktonic and benthic foraminiferal $\delta^{13}C$ values during the LGM compared to the Holocene is evident (Fig. 6 c; and Supplementary Fig. S5~~3~~), suggesting a more efficient BCP.

5.3 pCO_2 record of the BUS over the last 27 ka BP

Although $\delta^{11}B$ in foraminifera shells and $\delta^{13}C$ of alkenones are the most commonly applied methods to reconstruct pCO_2, these proxies are only very rarely compared in the same record. Since these proxies are recording different components of the speciation of carbon in seawater and have different biases, they not necessarily have to show similar results. Here, we observe only a modest change in pH (8.08-8.23, derived from foraminiferal $\delta^{11}B$) during the last deglaciation, whereas pCO_2 values show a change from 180 to 280 ppm (derived from $\delta^{13}C$ of alkenones) (Fig. 7).

Minor variability in pH was reported previously by Raitzsch et al. (2018) for the Walvis Ridge for the same time interval, although reconstructed pH values were slightly higher (0.10-0.14 pH units). Although only minor, the offset is in line with the core studied here being closer to the upwelling area, as the major upwelling area extends only about 200 km out of the coast today (Lutjeharms and Meeuwis, 1987; Lutjeharms and Stockton, 1987). With lowest pH values in the core of the upwelling area and values increasing towards the open ocean, the trend in the offset between the two areas is minor but in the right direction.

Using pH and total alkalinity, pCO_2 can be calculated, suggesting higher pCO_2 compared to the known atmospheric values over the past 27 ka BP (Fig. 7; Petit et al., 1999). Calculated pCO_2 based on the foraminiferal $\delta^{11}B$ only match seawater equilibrium values at 13.5 and 8.2 ka BP~~, corresponding to two major climate events (the Bølling-Allerød event and the 8.2 ka BP cooling event, respectively)~~, which is likely~~. Whereas the Bølling-Allerød event correspond~~related~~s to the ~~maximum~~ changes in AMOC intensity. Whereas the Bølling-Allerød event marks an AMOC amplification, ~~the 8.2 ka BP event is generally assumed to be associated to a reduced~~ AMOC was reduced around 8.2 ka BP due to the meltwater input in the North Atlantic (Matero et al., 2017; Barber et al., 1999; Pedro et al., 2016; Blunier et al., 1997). However, the calculated pCO_2 values are associated with considerable uncertainty for a large part related to total alkalinity being ill-constrained. Using estimates of total alkalinity based on relative sea level change is debated (e.g., De La Vega et al., 2023) as this does not account for all changes in alkalinity on glacial-interglacial timescales. Because total alkalinity calculated based on the relative sea level change during the last deglaciation results in only a small (less than 10 ppm) offset, we here used constant alkalinity (2349 ± 11 µmol kg^{-1}, GLODAPv2023; Lauvset et al., 2024) in combination with boron isotope-based pH to determine pCO_2. The trends observed here are not affected by the alkalinity values used.

The seawater pCO_2 reconstruction based on the $\delta^{13}C$ of alkenones follows past atmospheric pCO_2 known from the Vostok ice core record remarkably well (Petit et al., 1999). This suggests that over the interval studied here, this remained more or less in equilibrium with the atmosphere with regard to CO_2 and did not act as an appreciable source or sink. An offset is observed (about 65 ppm) during the Holocene, between 11 and 7 ka BP, when

alkenone-based reconstruction suggests somewhat lower pCO_2 values compared to the ice core record, although this difference falls well within the uncertainty of the proxy. This could indicate a temporary transition of the area to a CO_2 sink as the seawater becomes undersaturated with respect to CO_2.

The good agreement between alkenone-based and ice core pCO_2 records suggests that previously recognized complications in applying this proxy may not be relevant at this particular setting. Adaptation of CCM by the alkenone producers can hamper the use of the proxy under low pCO_2 conditions (Badger, 2021). However, the mechanisms that may control CCM in the alkenone producers are not fully constrained (e.g., Reinfelder, 2011), and effectiveness of the CCM may differ between species (e.g., Goudet et al., 2020; Heureux et al., 2017). As the reconstruction of pCO_2 values based on alkenone $\delta^{13}C$ provided a reasonable record here and in another upwelling region (Palmer et al., 2010), application of this proxy in upwelling sites may be able to rely on the classical concept of ~~Previous studies have observed discrepancy between alkenone based pCO_2 reconstruction and ice core records (Palmer et al., 2010; Andersen et al., 1999; Zhang et al., 2013; Witkowski et al., 2020; Jasper et al., 1994), which could be related to disequilibrium between sea surface and the atmosphere, especially at dynamic sites like upwelling regions. However, it may also be explained by the mechanism of CO_2 uptake in the algal cell. Current application of the alkenone pCO_2 proxy assumes the~~ passive diffusion of CO_2 (Bidigare et al., 1997; Laws et al., 1995). Additional uncertainty in the alkenone-based pCO_2 reconstruction may derive from the estimation of the *b* factor. ~~. However, much evidence indicates that alkenone producers adapted a carbon concentrating mechanism (CCM; Stoll et al., 2019; Reinfelder, 2011; Bolton and Stoll, 2013; Badger, 2021), which enables carbon acquisition in the cell through the active pumping of HCO_3^- to the chloroplast during low pCO_2 conditions. While such mechanism inevitably hampers the application of the pCO_2 proxy, efficiency of the CCM is potentially also affected by local conditions which may result in alkenone based pCO_2 reconstructions at some sites still being able to reproduce glacial atmospheric values . Furthermore, it has been shown that CCM's may induce their own isotopic fractionation .~~

~~Also, pCO_2 reconstructions based on alkenones $\delta^{13}C$ values are subject to uncertainties related to the *b* factor. The *b* value expresses the effect of multiple parameters related to the physiology of the alkenone producers (Jasper et al., 1994; Rau et al., 1996; Popp et al., 1998), which is best represented by a linear relationship to nutrient availability (Bidigare et al., 1997).~~ Often modern, constant, [PO_4^{3-}] is assumed to estimate the *b* factor for reconstructing pCO_2 (Pagani et al., 1999; Zhang et al., 2013; Pagani et al., 2005; Witkowski et al., 2020), or~~.~~ ~~A~~assuming that the membrane permeability has not changed significantly, one can correct for growth rate effects of the alkenone producers (Zhang et al., 2019; Zhang et al., 2020). Here, ~~W~~we ~~here relied on the analysis of~~used foraminiferal ~~-~~Ba/Ca, which ~~in planktonic foraminiferal shells as a proxy for seawater [PO_4^{3-}]. Ba/Ca~~ is suggested to reflect nutrient ([PO_4^{3-}]) variations ~~-~~but does not vary with temperature, salinity or carbon chemistry parameters (Lea and Spero, 1994; Hönisch et al., 2011) unlike other suggested nutrient proxies such as Cd/Ca (Oppo and Rosenthal, 1994; Allen et al., 2016) and Zn/Ca (Van Dijk et al., 2017). Thus, using this approach represents an efficient way to ~~tackle~~ address some of the uncertainties originating fr~~o~~om local conditions. ~~While uncertainties described for the above-mentioned factors may impact minor changes in the pCO_2 record, observed trends on glacial-interglacial timescales can be still interpreted.~~

Formatted: Font: Italic
Formatted: Subscript
Formatted: Font: Italic
Formatted: Subscript
Formatted: Font: Italic
Formatted: Subscript
Formatted: Superscript
Field Code Changed
Formatted: Font: Italic
Formatted: Subscript
Formatted: Subscript
Formatted: Superscript

Uncertainties in the different factors affecting pCO_2 estimates urge to develop additional independent carbon system parameter proxies that can supplement the $\delta^{11}B$-pH proxy. Among the six variables, the most commonly tackled parameter is $[CO_3^{2-}]$ using element / calcium ratios (El/Ca) such as B/Ca and more recently suggested S/Ca and S/Mg . Alternative foraminifera based pCO_2 reconstructions using core top calibrations for B/Ca and S/Mg are discussed in the Supplementary Material (Supplementary Text S1). Before unravelling differences in local carbon uptake and/or outgassing over glacial-interglacial cycles, it is important to decide which foraminifer-based proxy records best reflects local carbon speciation. Although using B/Ca (Supplementary Fig. S4) and S/Mg (Supplementary Fig. S5) bring alkenone and boron based pCO_2 reconstructions closer together, inherent error propagation also renders the records more difficult to differentiate. Hence, although we note the necessity and possibilities to improve B-isotope based pCO_2 reconstructions, we here base our down-core foraminifera based pCO_2 reconstruction on using boron isotopes only.

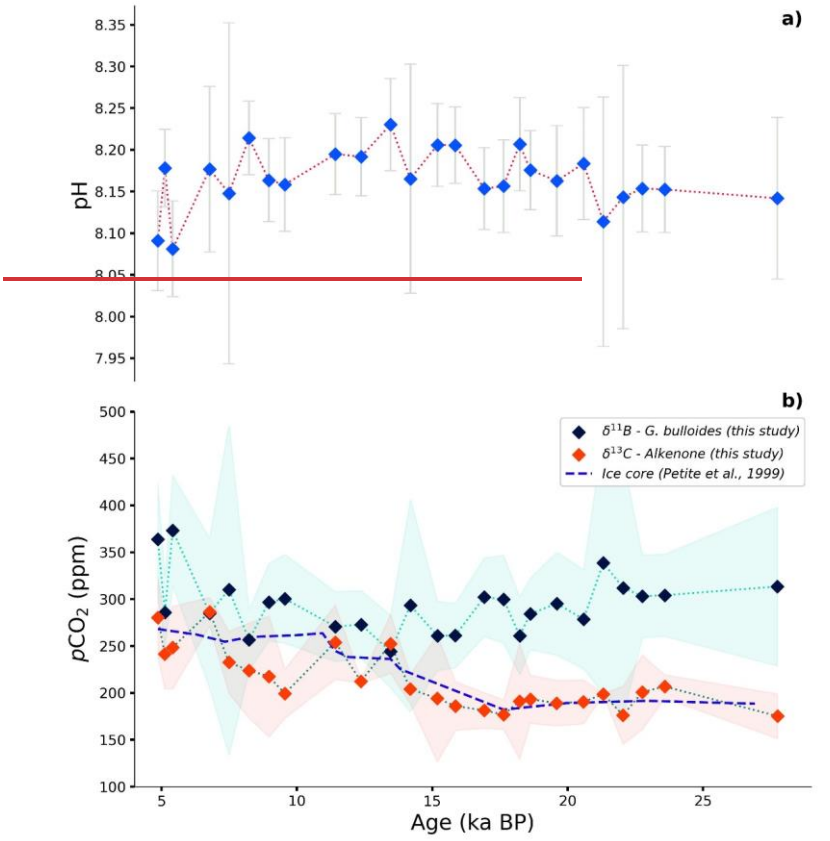
a)
pH
8.35
8.30
8.25
8.20
8.15
8.10
8.05
8.00
7.95
b)
$\delta^{11}B$ - G. bulloides (this study)
$\delta^{13}C$ - Alkenone (this study)
Ice core (Petite et al., 1999)
pCO_2 (ppm)
500
450
400
350
300
250
200
150
100
5
10
15
20
25
Age (ka BP)

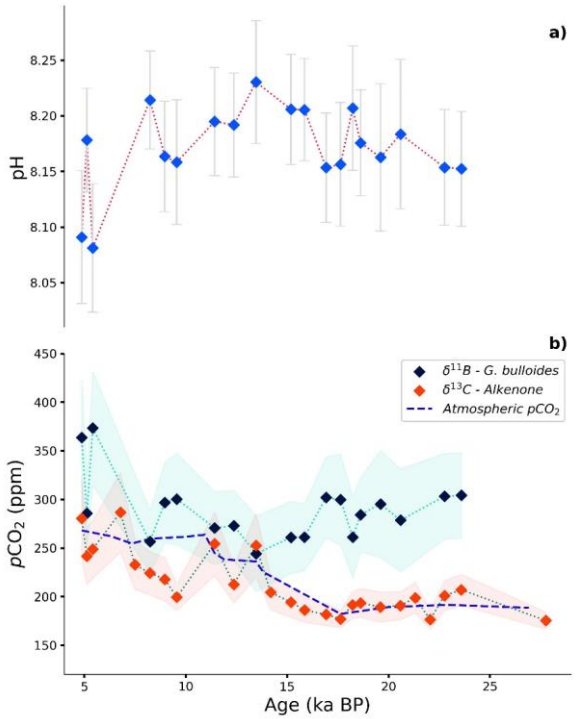

Figure 7: Reconstruction of a) pH based on $\delta^{11}B$ of *G. bulloides*, and b) pCO_2 based on $\delta^{11}B$ of *G. bulloides* combined with a constant total alkalinity value of 2349 ± 11.07 µmol kg^{-1} (dark blues diamonds) and $\delta^{13}C$ of alkenones (red diamonds). Modern day pCO_2 value of the AAIW is approximately 326 ppm (Lauvset et al., 2024; Salt et al., 2015). Blues dashed line shows the Vostok ice core record of pCO_2 (Petit et al., 1999). Light green and red shaded area represent propagated error for the foraminifera and alkenone based reconstructions, respectively. See further details on uncertainty propagation in the text.

Formatted: Font: Italic

5.4 Change in the efficiency of BCP and CO_2 disequilibrium

Most obvious from comparing the alkenone and foraminifera based pCO_2 reconstruction is the difference in amplitude of change on a glacial-interglacial time scale. Whereas the alkenone based reconstruction closely mimics atmospheric changes, the foraminifera-based reconstruction shows a constant pCO_2. Because the *G. bulloides* are proliferating during the upwelling season, they likely primarily reflect the somewhat deeper upwelled water compared to alkenones which are formed e.g., by the surface dwelling coccolithophorids. This implies more intense drawdown and recycling of CO_2 from the surface layers to the intermediate waters. The water upwelled in the BUS is AAIW and hence a relative increase in pCO_2 in the upwelled waters implies enhanced CO_2 storage in these waters.

Lower atmospheric CO_2 during the glacial is likely explained by multiple processes. The larger extent of sea ice over the glacial Southern Ocean prevented CO_2 escaping from seawater in an area today acting as a major CO_2 exchange region (Stephens and Keeling, 2000), whereas enhanced iron fertilization likely contributed to more efficient utilization and transport of carbon and nutrients to the deep (Martin, 1990; Martínez-García et al., 2014). Aeolian transport and dissolution in the shelf regions might have provided important sources of iron at that time (Martin, 1990; Tian et al., 2023), which ~~,~~ would locally influence air-sea carbon balance, still with minimum impact on global atmospheric pCO_2 due to adjacent regions where excess carbon can be utilized. Also locally at the BUS, aeolian transport presumably increased due to the intensified trade winds (Stuut et al., 2002), although a more humid climate may (Stuut et al., 2002; Cockcroft et al., 1987) or may not (Shi et al., 1998; Partridge et al., 1999) have prevailed in southwest Africa during the LGM. Although stronger winds may have provided sufficient iron for phytoplankton growth locally, excess iron input in the sub-Antarctic region most likely provided a much larger source for additional mid-depth CO_2 storage (Martínez-García et al., 2014). A more efficient biological carbon pump, as indicated by the offset between the planktonic and benthic foraminiferal carbon isotope records, suggest that an increased supply of carbon in the upwelling areas from intermediate depths to the surface, may have been effectively counterbalanced.

Concentrations of CO_2 in the ~~intermediate~~ subsurface waters show on average comparable values during the Holocene and LGM, and hence imply a difference in the pCO_2 gradients (ΔpCO_2 = $pCO_{2(\text{~~intermediate~~subsurface})}$ - $pCO_{2(\text{surface})}$) between the surface and subsurface (and intermediate) waters (Fig. 8). Note that *G. bulloides* may migrate between approximately 50 to 400 m, which can affect the calculated pCO_2 gradients. Still, *G. bulloides* represents a larger average depth than the alkenone-based record, and hence, carbon system conditions that are closer to those of the upwelled intermediate waters. Interglacial difference between alkenone and foraminifera-based reconstruction shows ΔpCO_2 value of about 6~~4~~2 ± 2~~9~~0 ppm, while during glacial times this difference increases to approximately ~~104~~ 94 ± 2~~9~~0 ppm. Atmospheric pCO_2 was significantly reduced during the LGM, hence the presence of an increased amount of CO_2 at ~~intermediate~~ subsurface depths implies either enhanced upwelling or that the upwelled waters were richer in CO_2 or both. Foraminifera-based proxies indicate more intense upwelling during glacial times (Oberhänsli, 1991; Little et al., 1997), but at the same time radiolarian based upwelling proxies suggest reduced upwelling (Des Combes and Abelmann, 2007). Due to its location and the influence of water masses both from the north and the south, cells of the BUS are characterized by different environmental conditions ~~(e.g., temperature and nutrients)~~(e.g., temperature and nutrients; Emeis et al., 2018). During the LGM, cold source waters likely impacted the northern cells of the BUS more than its central and southern parts (Des Combes and Abelmann, 2007) affirming complexity of this upwelling system. While we may conclude that upwelling intensities were different from one cell to another, potentially also impacted by the offshore transition of the modern strong upwelling cells (e.g., Mollenhauer et al., 2002), increased cold water input does not necessarily correlate with stronger upwelling (Des Combes and Abelmann, 2007), potentially explaining conflicting interpretations.

Formatted: Font: Italic
Formatted: Subscript
Formatted: Font: Italic
Formatted: Font: Italic
Formatted: Subscript
Formatted: Font: Italic

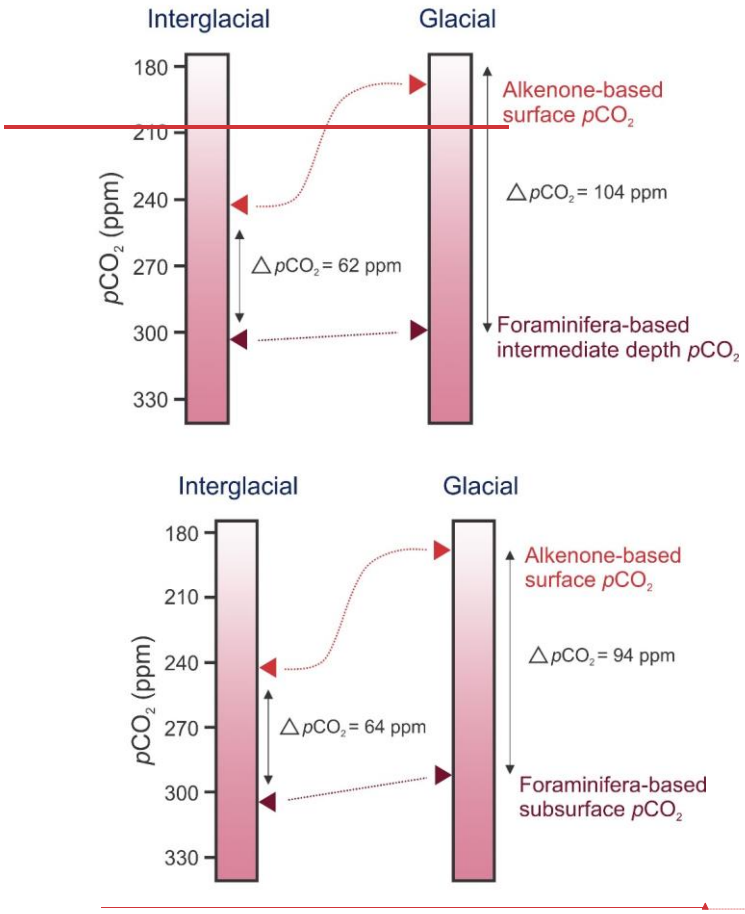

Figure 8: Schematic comparison of interglacial and glacial pCO_2 values. Red arrows mark average interglacial and glacial values calculated from the alkenone and planktonic foraminifera (pH and total alkalinity) based proxies of this study.

Based on comparing pCO_2 proxies, with *G. bulloides* recording primarily the upwelled waters and alkenones the surface waters, we see evidence for enhanced storage of carbon at depth during the glacial. This is in line with the reconstructed high productivity on the basis of elevated iron input in the high nutrient, low chlorophyll (HNLC) areas at that time in the sub-Antarctic region (Martínez-García et al., 2014). The resulting mid depth high CO_2 waters provide also at that time the source for upwelled waters in the BUS, which could have resulted in the local release of (part of the) stored CO_2 if not prevented by an efficient biological carbon pump. If iron input was enhanced also locally (Stuut et al., 2002), this could increase the biological pump, which then acted as an effective cap on the stored carbon. Both remote and local enhanced iron supplies hence contributed to ~~lowering atmospheric~~preventing the release of mid-depth ~~p~~CO_2 during the glacial.

Formatted: Dutch (Netherlands)

Formatted: English (United Kingdom)

6 Conclusions

Carbon system proxies were applied to demonstrate changes in inorganic carbon chemistry of the Northern Benguela Upwelling System over the last 27 ka BP. Temperature reconstructions based on both organic and inorganic proxies indicate that the BUS ~~is generally~~may be associated to climatic changes observed both in the Northern and Southern Hemisphere. While surface values of pCO_2 reconstructed from $\delta^{13}C$ of alkenones follow atmospheric changes of pCO_2 remarkably well, the foraminifera-based reconstruction~~s~~ suggest~~s~~ minor variation in pCO_2 ~~at intermediate depth~~in the subsurface since the L~~l~~ast G~~g~~lacial M~~m~~aximum until present. Hence, the increased gradient of pCO_2 between the surface waters and depth observed for the last glacial period provide evidence for enhanced storage of carbon in the Antarctic Intermediate Waters. Outgassing of CO_2, however, could be effectively prevented by the biological carbon pump as also indicated by the offset in the $\delta^{13}C$ of planktonic and benthic foraminifera.

Formatted: Dutch (Netherlands)

Formatted: Dutch (Netherlands)

Data availability

All data used in this study can be obtained from the NIOZ Data Archive System at https://doi.org/10.25850/nioz/7b.b.lh ~~https://doi.org/10.25850/nioz/7b.b.lh~~ (Karancz et al., 2024): Table 1. Uncalibrated and calibrated radiocarbon ages; Table 2. Single foraminifera analysis (LA-Q-ICP-MS); Table 3. $\delta^{18}O$ and $\delta^{13}C$ of planktonic and benthic foraminifera, El/Ca and $\delta^{11}B$ of planktonic foraminifera, $U^{K'}_{37}$ and $\delta^{13}C$ of alkenones; Table 4. XRF and lightness reflectance data.~~.~~

Author contributions

SK, LJdN, SS, GJR designed the study. RH and ZE collected the sample material and SK prepared and processed the samples. SK, BwdW, MTJvdM, SM were responsible for the analysis of foraminifera and alkenones. JL and NH conducted the radiocarbon analysis. SK interpreted and visualized the data under the supervision of LJdN, SS, GJR and drafted the paper with contribution from all co-authors.

Competing interests

The authors declare that they have no conflict of interest.

Acknowledgement

This work was carried out under the program of the Netherlands Earth System Science Centre (NESSC), financially supported by the Ministry of Education, Culture and Science (OCW) and the European Union's Horizon 2020 research and innovation program under the Marie Skłodowska-Curie grant with agreement No. [847504]. We thank Wim Boer, Piet van Gaever, Patrick Laan, Jort Ossebaar, Anchelique Mets, and the laboratory of Ion-Beam Physics at ETH Zurich for the technical support during sample preparations and the geochemical analysis.

References

Alldredge, A. L. and Silver, M. W.: Characteristics, dynamics and significance of marine snow, Prog. Oceanogr., 20, 41-82, https://doi.org/10.1016/0079-6611(88)90053-5, 1988.

Allen, K. A., Hönisch, B., Eggins, S. M., Haynes, L. L., Rosenthal, Y., and Yu, J.: Trace element proxies for surface ocean conditions: A synthesis of culture calibrations with planktic foraminifera, Geochim. Cosmochim. Acta, 193, 197-221, https://doi.org/10.1016/j.gca.2016.08.015, 2016.

Alley, R. B.: The Younger Dryas cold interval as viewed from central Greenland, Quat. Sci. Rev., 19, 213-226, https://doi.org/10.1016/S0277-3791(99)00062-1, 2000.

Andersen, N., Müller, P. J., Kirst, G., and Schneider, R. R.: Alkenone δ^{13}C as a Proxy for Past *P*CO_2 in Surface Waters: Results from the Late Quaternary Angola Current, in: Use of Proxies in Paleoceanography: Examples from the South Atlantic, edited by: Fischer, G., and Wefer, G., Springer Berlin Heidelberg, Berlin, Heidelberg, 469-488, https://doi.org/10.1007/978-3-642-58646-0_19, 1999.

Armstrong, R. A., Lee, C., Hedges, J. I., Honjo, S., and Wakeham, S. G.: A new, mechanistic model for organic carbon fluxes in the ocean based on the quantitative association of POC with ballast minerals, Deep Sea Research Part II: Topical Studies in Oceanography, 49, 219-236, https://doi.org/10.1016/S0967-0645(01)00101-1, 2001.

Badger, M. P. S.: Alkenone isotopes show evidence of active carbon concentrating mechanisms in coccolithophores as aqueous carbon dioxide concentrations fall below 7 µmol L^{-1}, Biogeosciences, 18, 1149-1160, https://doi.org/10.5194/bg-18-1149-2021, 2021.

Bae, S. W., Lee, K. E., and Kim, K.: Use of carbon isotopic composition of alkenone as a CO_2 proxy in the East Sea/Japan Sea, Continental Shelf Research, 107, 24-32, https://doi.org/10.1016/j.csr.2015.07.010, 2015.

Barber, D. C., Dyke, A., Hillaire-Marcel, C., Jennings, A. E., Andrews, J. T., Kerwin, M. W., Bilodeau, G., McNeely, R., Southon, J., Morehead, M. D., and Gagnon, J. M.: Forcing of the cold event of 8,200 years ago by catastrophic drainage of Laurentide lakes, Nature, 400, 344-348, https://doi.org/10.1038/22504, 1999.

Barker, S., Greaves, M., and Elderfield, H.: A study of cleaning procedures used for foraminiferal Mg/Ca paleothermometry, Geochem. Geophys. Geosyst., 4, https://doi.org/10.1029/2003GC000559, 2003.

Bemis, B. E., Spero, H. J., Lea, D. W., and Bijma, J.: Temperature influence on the carbon isotopic composition of *Globigerina bulloides* and *Orbulina universa* (planktonic foraminifera), Mar. Micropaleontol., 38, 213-228, https://doi.org/10.1016/S0377-8398(00)00006-2, 2000.

Bice, K. L., Birgel, D., Meyers, P. A., Dahl, K. A., Hinrichs, K.-U., and Norris, R. D.: A multiple proxy and model study of Cretaceous upper ocean temperatures and atmospheric CO_2 concentrations, Paleoceanography, 21, https://doi.org/10.1029/2005PA001203, 2006.

Bidigare, R. R., Fluegge, A., Freeman, K. H., Hanson, K. L., Hayes, J. M., Hollander, D., Jasper, J. P., King, L. L., Laws, E. A., and Milder, J.: Consistent fractionation of ^{13}C in nature and in the laboratory: Growth-rate effects in some haptophyte algae, Global Biogeochem. Cycles, 11, 279-292, https://doi.org/10.1029/96GB03939, 1997.

Bijl, P. K., Houben, A. J. P., Schouten, S., Bohaty, S. M., Sluijs, A., Reichart, G.-J., Sinninghe Damsté, J. S., and Brinkhuis, H.: Transient Middle Eocene atmospheric CO_2 and temperature variations, Science, 330, 819-821, https://doi.org/10.1126/science.1193654, 2010.

Bijma, J., Spero, H., and Lea, D.: Reassessing foraminiferal stable isotope geochemistry: Impact of the oceanic carbonate system (experimental results), in: Fischer, G., Wefer, G. (eds) Use of proxies in paleoceanography, Springer, Berlin, Heidelberg, 489-512, https://doi.org/10.1007/978-3-642-58646-0_20, 1999.

Bird, C., Darling, K. F., Russell, A. D., Davis, C. V., Fehrenbacher, J., Free, A., Wyman, M., and Ngwenya, B. T.: Cyanobacterial endobionts within a major marine planktonic calcifier

Formatted: Font: (Default) Times New Roman

Formatted: Line spacing: Multiple 1.15 li

Formatted: Font: (Default) Times New Roman

Formatted: Font: (Default) Times New Roman

Formatted: Font: (Default) Times New Roman

Formatted: Font: (Default) Times New Roman

Formatted: Font: (Default) Times New Roman

Formatted: Font: (Default) Times New Roman

Formatted: Font: (Default) Times New Roman

Formatted: Font: (Default) Times New Roman

Formatted: Font: (Default) Times New Roman

Formatted: Font: (Default) Times New Roman

Formatted: Font: (Default) Times New Roman

Formatted: Font: (Default) Times New Roman

Formatted: Font: (Default) Times New Roman

Formatted: Font: (Default) Times New Roman

Formatted: Font: (Default) Times New Roman

Formatted: Font: (Default) Times New Roman

Formatted: Font: (Default) Times New Roman

Formatted: Font: (Default) Times New Roman

Formatted: Font: (Default) Times New Roman

Formatted: Font: (Default) Times New Roman

Formatted: Font: (Default) Times New Roman

Formatted: Font: (Default) Times New Roman

Formatted: Font: (Default) Times New Roman

Formatted: Font: (Default) Times New Roman

Formatted: Font: (Default) Times New Roman

Formatted: Font: (Default) Times New Roman

Formatted: Font: (Default) Times New Roman

Formatted: Font: (Default) Times New Roman

Formatted: Font: (Default) Times New Roman

Formatted: Font: (Default) Times New Roman

(*Globigerina bulloides*, Foraminifera) revealed by 16S rRNA metabarcoding, Biogeosciences, 14, 901-920, https://doi.org/10.5194/bg-14-901-2017, 2017.

Blaauw, M. and Christen, J. A.: Flexible paleoclimate age-depth models using an autoregressive gamma process, Bayesian Analysis, 6, 457-474, 418, https://doi.org/10.1214/11-BA618, 2011.

Blunier, T. and Brook, E. J.: Timing of Millennial-Scale Climate Change in Antarctica and Greenland During the Last Glacial Period, Science, 291, 109-112, https://doi.org/10.1126/science.291.5501.109, 2001.

Blunier, T., Schwander, J., Stauffer, B., Stocker, T., Dällenbach, A., Indermühle, A., Tschumi, J., Chappellaz, J., Raynaud, D., and Barnola, J. M.: Timing of the Antarctic cold reversal and the atmospheric CO_2 increase with respect to the Younger Dryas Event, Geophys. Res. Lett., 24, 2683-2686, https://doi.org/10.1029/97GL02658, 1997.

Boer, W., Nordstad, S., Weber, M., Mertz-Kraus, R., Hönisch, B., Bijma, J., Raitzsch, M., Wilhelms-Dick, D., Foster, G. L., and Goring-Harford, H.: New calcium carbonate nano-particulate pressed powder pellet (NFHS-2-NP) for LA-ICP-OES, LA-(MC)-ICP-MS and µXRF, Geostand. Geoanalytical Res., 46, 411-432, https://doi.org/10.1111/ggr.12425, 2022.

Bolton, C. T. and Stoll, H. M.: Late Miocene threshold response of marine algae to carbon dioxide limitation, Nature, 500, 558-562, https://doi.org/10.1038/nature12448, 2013.

Bond, G., Broecker, W., Johnsen, S., McManus, J., Labeyrie, L., Jouzel, J., and Bonani, G.: Correlations between climate records from North Atlantic sediments and Greenland ice, Nature, 365, 143-147, https://doi.org/10.1038/365143a0, 1993.

Brady, R. X., Lovenduski, N. S., Alexander, M. A., Jacox, M., and Gruber, N.: On the role of climate modes in modulating the air–sea CO_2 fluxes in eastern boundary upwelling systems, Biogeosciences, 16, 329-346, https://doi.org/10.5194/bg-16-329-2019, 2019.

Broecker, W. S.: Paleocean circulation during the last deglaciation: a bipolar seesaw?, Paleoceanography, 13, 119-121, https://doi.org/10.1029/97PA03707, 1998.

Cacho, I., Grimalt, J. O., Pelejero, C., Canals, M., Sierro, F. J., Flores, J. A., and Shackleton, N.: Dansgaard-Oeschger and Heinrich event imprints in Alboran Sea paleotemperatures, Paleoceanography, 14, 698-705, https://doi.org/10.1029/1999PA900044, 1999.

Calvo, E., Pelejero, C., De Deckker, P., and Logan, G. A.: Antarctic deglacial pattern in a 30 kyr record of sea surface temperature offshore South Australia, Geophys. Res. Lett., 34, https://doi.org/10.1029/2007GL029937, 2007.

Carr, M.-E.: Estimation of potential productivity in Eastern Boundary Currents using remote sensing, Deep Sea Research Part II: Topical Studies in Oceanography, 49, 59-80, https://doi.org/10.1016/S0967-0645(01)00094-7, 2001.

Chanakya, I. V. S. and Misra, S.: Accurate and precise determination of the boron isotope ratio by QQQ-ICP-MS: application to natural waters and carbonates, J. Anal. At. Spectrom., 37, 1327-1339, https://doi.org/10.1039/D2JA00051B, 2022.

Charles, C. D. and Morley, J. J.: The paleoceanographic significance of the radiolarian didymocyrtis tetrathalamus in Eastern Cape basin sediments, Palaeogeogr., Palaeoclimatol., Palaeoecol., 66, 113-126, https://doi.org/10.1016/0031-0182(88)90084-3, 1988.

Chavez, F. P. and Messié, M.: A comparison of eastern boundary upwelling ecosystems, Prog. Oceanogr., 83, 80-96, https://doi.org/10.1016/j.pocean.2009.07.032, 2009.

Clark, P. U., Dyke, A. S., Shakun, J. D., Carlson, A. E., Clark, J., Wohlfarth, B., Mitrovica, J. X., Hostetler, S. W., and McCabe, A. M.: The Last Glacial Maximum, Science, 325, 710-714, https://doi.org/10.1126/science.1172873, 2009.

Cockcroft, M. J., Wilkinson, M. J., and Tyson, P. D.: The application of a present-day climatic model to the late quaternary in southern Africa, Clim. Change, 10, 161-181, https://doi.org/10.1007/BF00140253, 1987.

Formatted: Font: (Default) Times New Roman

Conte, M., Volkman, J., and Eglinton, G.: Lipid biomarkers of the Haptophyta, in: Green, JC and Leadbeater, BSC (eds) The haptophyte algae, Clarendon Press: Oxford, 1994.

Conte, M. H., Sicre, M.-A., Rühlemann, C., Weber, J. C., Schulte, S., Schulz-Bull, D., and Blanz, T.: Global temperature calibration of the alkenone unsaturation index ($U^{K'}_{37}$) in surface waters and comparison with surface sediments, Geochem. Geophys. Geosyst., 7, https://doi.org/10.1029/2005GC001054, 2006.

Curry, W. B. and Oppo, D. W.: Glacial water mass geometry and the distribution of $\delta^{13}C$ of ΣCO_2 in the western Atlantic Ocean, Paleoceanography, 20, https://doi.org/10.1029/2004PA001021, 2005.

Damsté, J. S. S., Kuypers, M. M. M., Pancost, R. D., and Schouten, S.: The carbon isotopic response of algae, (cyano)bacteria, archaea and higher plants to the late Cenomanian perturbation of the global carbon cycle: Insights from biomarkers in black shales from the Cape Verde Basin (DSDP Site 367), Org. Geochem., 39, 1703-1718, https://doi.org/10.1016/j.orggeochem.2008.01.012, 2008.

Davis, C. V., Fehrenbacher, J. S., Benitez-Nelson, C., and Thunell, R. C.: Trace element heterogeneity across individual planktic foraminifera from the modern Cariaco Basin, Journal of Foraminiferal Research, 50, 204-218, https://doi.org/10.2113/gsjfr.50.2.204, 2020.

De La Rocha, C. L. and Passow, U.: Factors influencing the sinking of POC and the efficiency of the biological carbon pump, Deep Sea Research Part II: Topical Studies in Oceanography, 54, 639-658, https://doi.org/10.1016/j.dsr2.2007.01.004, 2007.

de la Vega, E., Chalk, T. B., Hain, M. P., Wilding, M. R., Casey, D., Gledhill, R., Luo, C., Wilson, P. A., and Foster, G. L.: Orbital CO_2 reconstruction using boron isotopes during the late Pleistocene, an assessment of accuracy, Clim. Past, 19, 2493-2510, https://doi.org/10.5194/cp-19-2493-2023, 2023.

de Nooijer, L. J., Spero, H., Erez, J., Bijma, J., and Reichart, G.-J.: Biomineralization in perforate foraminifera, Earth-Sci. Rev., 135, 48-58, https://doi.org/10.1016/j.earscirev.2014.03.013, 2014.

de Villiers, S., Greaves, M., and Elderfield, H.: An intensity ratio calibration method for the accurate determination of Mg/Ca and Sr/Ca of marine carbonates by ICP-AES, Geochem. Geophys. Geosyst., 3, https://doi.org/10.1029/2001GC000169, 2002.

Degens, E. T., Guillard, R. R. L., Sackett, W. M., and Hellebust, J. A.: Metabolic fractionation of carbon isotopes in marine plankton—I. Temperature and respiration experiments, Deep Sea Research and Oceanographic Abstracts, 15, 1-9, https://doi.org/10.1016/0011-7471(68)90024-7, 1968.

Dekens, P. S., Lea, D. W., Pak, D. K., and Spero, H. J.: Core top calibration of Mg/Ca in tropical foraminifera: Refining paleotemperature estimation, Geochem. Geophys. Geosyst., 3, 1-29, https://doi.org/10.1029/2001GC000200, 2002.

Denton, G. H., Anderson, R. F., Toggweiler, J. R., Edwards, R. L., Schaefer, J. M., and Putnam, A. E.: The Last Glacial Termination, Science, 328, 1652-1656, https://doi.org/10.1126/science.1184119, 2010.

Des Combes, H. J. and Abelmann, A.: A 350-ky radiolarian record off Lüderitz, Namibia—evidence for changes in the upwelling regime, Mar. Micropaleontol., 62, 194-210, https://doi.org/10.1016/j.marmicro.2006.08.004, 2007.

DeVries, T. and Weber, T.: The export and fate of organic matter in the ocean: New constraints from combining satellite and oceanographic tracer observations, Global Biogeochem. Cycles, 31, 535-555, https://doi.org/10.1002/2016GB005551, 2017.

Dewar, G., Reimer, P. J., Sealy, J., and Woodborne, S.: Late-Holocene marine radiocarbon reservoir correction (ΔR) for the west coast of South Africa, The Holocene, 22, 1481-1489, https://doi.org/10.1177/09596836124497, 2012.

Formatted: Font: (Default) Times New Roman

Dickson, A. G.: Thermodynamics of the dissociation of boric acid in synthetic seawater from 273.15 to 318.15 K, Deep Sea Research Part A. Oceanographic Research Papers, 37, 755-766, https://doi.org/10.1016/0198-0149(90)90004-F, 1990.

Diester-Haass, L., Meyers, P. A., and Rothe, P.: The Benguela Current and associated upwelling on the southwest African Margin: a synthesis of the Neogene-Quaternary sedimentary record at DSDP sites 362 and 532, Geological Society, London, Special Publications, 64, 331-342, https://doi.org/10.1144/GSL.SP.1992.064.01.2, 1992.

Ducklow, H. W., Steinberg, D. K., and Buesseler, K. O.: Upper ocean carbon export and the biological pump, Oceanography, 14, 50-58, 2001.

Dueñas-Bohórquez, A., da Rocha, R. E., Kuroyanagi, A., Bijma, J., and Reichart, G.-J.: Effect of salinity and seawater calcite saturation state on Mg and Sr incorporation in cultured planktonic foraminifera, Mar. Micropaleontol., 73, 178-189, https://doi.org/10.1016/j.marmicro.2009.09.002, 2009.

Emeis, K., Eggert, A., Flohr, A., Lahajnar, N., Nausch, G., Neumann, A., Rixen, T., Schmidt, M., Van der Plas, A., and Wasmund, N.: Biogeochemical processes and turnover rates in the Northern Benguela Upwelling System, Journal of Marine Systems, 188, 63-80, https://doi.org/10.1016/j.jmarsys.2017.10.001, 2018.

Erez, J.: The source of ions for biomineralization in foraminifera and their implications for paleoceanographic proxies, Rev. Mineral. Geochem., 54, 115-149, https://doi.org/10.2113/0540115, 2003.

Fahrni, S. M., Wacker, L., Synal, H. A., and Szidat, S.: Improving a gas ion source for ^{14}C AMS, Nuclear Instruments and Methods in Physics Research Section B: Beam Interactions with Materials and Atoms, 294, 320-327, https://doi.org/10.1016/j.nimb.2012.03.037, 2013.

Flores, J.-A., Gersonde, R., and Sierro, F. J.: Pleistocene fluctuations in the Agulhas Current Retroflection based on the calcareous plankton record, Mar. Micropaleontol., 37, 1-22, https://doi.org/10.1016/S0377-8398(99)00012-2, 1999.

Foster, G. L. and Rae, J. W.: Reconstructing ocean pH with boron isotopes in foraminifera, Annu. Rev. Earth Planet. Sci., 44, 207-237, https://doi.org/10.1146/annurev-earth-060115-012226, 2016.

Foster, G. L., Pogge von Strandmann, P. A. E., and Rae, J. W. B.: Boron and magnesium isotopic composition of seawater, Geochem. Geophys. Geosyst., 11, https://doi.org/10.1029/2010GC003201, 2010.

Fowler, S. W. and Knauer, G. A.: Role of large particles in the transport of elements and organic compounds through the oceanic water column, Prog. Oceanogr., 16, 147-194, https://doi.org/10.1016/0079-6611(86)90032-7, 1986.

Francois, R., Honjo, S., Krishfield, R., and Manganini, S.: Factors controlling the flux of organic carbon to the bathypelagic zone of the ocean, Global Biogeochem. Cycles, 16, 34-31-34-20, https://doi.org/10.1029/2001GB001722, 2002.

Franzese, A. M., Hemming, S. R., Goldstein, S. L., and Anderson, R. F.: Reduced Agulhas Leakage during the Last Glacial Maximum inferred from an integrated provenance and flux study, Earth. Planet. Sci. Lett., 250, 72-88, https://doi.org/10.1016/j.epsl.2006.07.002, 2006.

Gaillardet, J., Lemarchand, D., Göpel, C., and Manhès, G.: Evaporation and sublimation of boric acid: Application for boron purification from organic rich solutions, Geostandards Newsletter, 25, 67-75, https://doi.org/10.1111/j.1751-908X.2001.tb00788.x, 2001.

Gordon, A. L.: Interocean exchange of thermocline water, J. Geophys. Res. Oceans, 91, 5037-5046, https://doi.org/10.1029/JC091iC04p05037, 1986.

Goudet, M. M., Orr, D. J., Melkonian, M., Müller, K. H., Meyer, M. T., Carmo-Silva, E., and Griffiths, H.: Rubisco and carbon-concentrating mechanism co-evolution across chlorophyte and streptophyte green algae, New Phytol., 227, 810-823, https://doi.org/10.1111/nph.16577, 2020.

Formatted: Font: (Default) Times New Roman

Gray, W. R. and Evans, D.: Nonthermal influences on Mg/Ca in planktonic foraminifera: A review of culture studies and application to the last glacial maximum, Paleoceanogr. Paleoclimatol., 34, 306-315, https://doi.org/10.1029/2018PA003517, 2019.

Gray, W. R., Weldeab, S., Lea, D. W., Rosenthal, Y., Gruber, N., Donner, B., and Fischer, G.: The effects of temperature, salinity, and the carbonate system on Mg/Ca in *Globigerinoides ruber* (white): A global sediment trap calibration, Earth. Planet. Sci. Lett., 482, 607-620, https://doi.org/10.1016/j.epsl.2017.11.026, 2018.

Gregor, L. and Monteiro, P. M.: Is the southern Benguela a significant regional sink of CO_2?, South African Journal of Science, 109, 1-5, https://doi.org/10.10520/EJC136398, 2013.

Gruber, N., Gloor, M., Mikaloff Fletcher, S. E., Doney, S. C., Dutkiewicz, S., Follows, M. J., Gerber, M., Jacobson, A. R., Joos, F., and Lindsay, K.: Oceanic sources, sinks, and transport of atmospheric CO_2, Global Biogeochem. Cycles, 23, https://doi.org/10.1029/2008GB003349, 2009.

Gu, S., Liu, Z., Zhang, J., Rempfer, J., Joos, F., and Oppo, D. W.: Coherent response of Antarctic Intermediate Water and Atlantic Meridional Overturning Circulation during the last deglaciation: Reconciling contrasting neodymium isotope reconstructions from the tropical Atlantic, Paleoceanography, 32, 1036-1053, https://doi.org/10.1002/2017PA003092, 2017.

Hain, M. P., Sigman, D., and Haug, G.: The biological pump in the past, Reference Module in Earth Systems and Environmental Sciences, Treatise on Geochemistry (Second Edition), The Oceans and Marine Geochemistry, 8, 485-517, https://doi.org/10.1016/B978-0-08-095975-7.00618-5, 2014.

Hales, B., Takahashi, T., and Bandstra, L.: Atmospheric CO_2 uptake by a coastal upwelling system, Global Biogeochem. Cycles, 19, https://doi.org/10.1029/2004GB002295, 2005.

Hart, T. J. and Currie, R. I.: The benguela current, 31, 1960.

Hayes, J. M.: Factors controlling ^{13}C contents of sedimentary organic compounds: Principles and evidence, Mar. Geol., 113, 111-125, https://doi.org/10.1016/0025-3227(93)90153-M, 1993.

Heaton, T. J., Köhler, P., Butzin, M., Bard, E., Reimer, R. W., Austin, W. E. N., Bronk Ramsey, C., Grootes, P. M., Hughen, K. A., Kromer, B., Reimer, P. J., Adkins, J., Burke, A., Cook, M. S., Olsen, J., and Skinner, L. C.: Marine20—The Marine Radiocarbon Age Calibration Curve (0–55,000 cal BP), Radiocarbon, 62, 779-820, https://doi.org/10.1017/RDC.2020.68, 2020.

Hemleben, C., Spindler, M., and Anderson, O. R.: Modern planktonic foraminifera, Springer-Verlag, New York1989.

Hemming, N. and Hanson, G.: Boron isotopic composition and concentration in modern marine carbonates, Geochim. Cosmochim. Acta, 56, 537-543, https://doi.org/10.1016/0016-7037(92)90151-8, 1992.

Henehan, M. J., Foster, G. L., Bostock, H. C., Greenop, R., Marshall, B. J., and Wilson, P. A.: A new boron isotope-pH calibration for Orbulina universa , with implications for understanding and accounting for 'vital effects', Earth. Planet. Sci. Lett., 454, 282-292, https://doi.org/10.1016/j.epsl.2016.09.024, 2016.

Henehan, M. J., Rae, J. W. B., Foster, G. L., Erez, J., Prentice, K. C., Kucera, M., Bostock, H. C., Martínez-Botí, M. A., Milton, J. A., Wilson, P. A., Marshall, B. J., and Elliott, T.: Calibration of the boron isotope proxy in the planktonic foraminifera *Globigerinoides ruber* for use in palaeo-CO_2 reconstruction, Earth. Planet. Sci. Lett., 364, 111-122, https://doi.org/10.1016/j.epsl.2012.12.029, 2013.

Henson, S. A., Sanders, R., Madsen, E., Morris, P. J., Le Moigne, F., and Quartly, G. D.: A reduced estimate of the strength of the ocean's biological carbon pump, Geophys. Res. Lett., 38, https://doi.org/10.1029/2011GL046735, 2011.

Formatted: Font: (Default) Times New Roman

Heureux, A. M. C., Young, J. N., Whitney, S. M., Eason-Hubbard, M. R., Lee, R. B. Y., Sharwood, R. E., and Rickaby, R. E. M.: The role of Rubisco kinetics and pyrenoid morphology in shaping the CCM of haptophyte microalgae, J. Exp. Bot., 68, 3959-3969, https://doi.org/10.1093/jxb/erx179, 2017.

Hill, A. E.: Eastern Ocean Boundaries, The Sea, VII, 29-67, 1998.

Hilting, A. K., Kump, L. R., and Bralower, T. J.: Variations in the oceanic vertical carbon isotope gradient and their implications for the Paleocene-Eocene biological pump, Paleoceanography, 23, https://doi.org/10.1029/2007PA001458, 2008.

Hodell, D. A., Nicholl, J. A., Bontognali, T. R. R., Danino, S., Dorador, J., Dowdeswell, J. A., Einsle, J., Kuhlmann, H., Martrat, B., Mleneck-Vautravers, M. J., Rodríguez-Tovar, F. J., and Röhl, U.: Anatomy of Heinrich Layer 1 and its role in the last deglaciation, Paleoceanography, 32, 284-303, https://doi.org/10.1002/2016PA003028, 2017.

Hönisch, B. and Hemming, N. G.: Ground-truthing the boron isotope-paleo-pH proxy in planktonic foraminifera shells: Partial dissolution and shell size effects, Paleoceanography, 19, https://doi.org/10.1029/2004PA001026, 2004.

Hönisch, B., Allen, K. A., Russell, A. D., Eggins, S. M., Bijma, J., Spero, H. J., Lea, D. W., and Yu, J.: Planktic foraminifers as recorders of seawater Ba/Ca, Mar. Micropaleontol., 79, 52-57, https://doi.org/10.1016/j.marmicro.2011.01.003, 2011.

Hover, V. C., Walter, L. M., and Peacor, D. R.: Early marine diagenesis of biogenic aragonite and Mg-calcite: new constraints from high-resolution STEM and AEM analyses of modern platform carbonates, Chem. Geol., 175, 221-248, https://doi.org/10.1016/S0009-2541(00)00326-0, 2001.

Howe, J. N. W., Piotrowski, A. M., Oppo, D. W., Huang, K.-F., Mulitza, S., Chiessi, C. M., and Blusztajn, J.: Antarctic intermediate water circulation in the South Atlantic over the past 25,000 years, Paleoceanography, 31, 1302-1314, https://doi.org/10.1002/2016PA002975, 2016.

Hughes, P. D., Gibbard, P. L., and Ehlers, J.: Timing of glaciation during the last glacial cycle: evaluating the concept of a global 'Last Glacial Maximum' (LGM), Earth-Sci. Rev., 125, 171-198, https://doi.org/10.1016/j.earscirev.2013.07.003, 2013.

Humphreys, M. P., Lewis, E. R., Sharp, J. D., and Pierrot, D.: PyCO2SYS v1. 8: marine carbonate system calculations in Python, Geoscientific Model Development, 15, 15-43, https://doi.org/10.5194/gmd-15-15-2022, 2022.

Jasper, J. P. and Hayes, J. M.: A carbon isotope record of CO_2 levels during the late Quaternary, Nature, 347, 462-464, https://doi.org/10.1038/347462a0, 1990.

Jasper, J. P., Hayes, J., Mix, A. C., and Prahl, F. G.: Photosynthetic fractionation of ^{13}C and concentrations of dissolved CO_2 in the central equatorial Pacific during the last 255,000 years, Paleoceanography, 9, 781-798, https://doi.org/10.1029/94PA02116, 1994.

Jouzel, J., Masson-Delmotte, V., Cattani, O., Dreyfus, G., Falourd, S., Hoffmann, G., Minster, B., Nouet, J., Barnola, J. M., Chappellaz, J., Fischer, H., Gallet, J. C., Johnsen, S., Leuenberger, M., Loulergue, L., Luethi, D., Oerter, H., Parrenin, F., Raisbeck, G., Raynaud, D., Schilt, A., Schwander, J., Selmo, E., Souchez, R., Spahni, R., Stauffer, B., Steffensen, J. P., Stenni, B., Stocker, T. F., Tison, J. L., Werner, M., and Wolff, E. W.: Orbital and Millennial Antarctic Climate Variability over the Past 800,000 Years, Science, 317, 793-796, https://doi.org/10.1126/science.1141038, 2007.

Kahn, M.: Non-equilibrium oxygen and carbon isotopic fractionation in tests of living planktonic-foraminifera, Oceanol. Acta, 2, 195-208, 1979.

Formatted: Font: (Default) Times New Roman

Kahn, M. I. and Williams, D. F.: Oxygen and carbon isotopic composition of living planktonic foraminifera from the northeast Pacific Ocean, Palaeogeogr., Palaeoclimatol., Palaeoecol., 33, 47-69, https://doi.org/10.1016/0031-0182(81)90032-8, 1981.

Kämpf, J. and Chapman, P.: Upwelling systems of the world, Springer Cham, https://doi.org/10.1007/978-3-319-42524-5, 2016.

Kaplan, M. R., Schaefer, J. M., Denton, G. H., Barrell, D. J. A., Chinn, T. J. H., Putnam, A. E., Andersen, B. G., Finkel, R. C., Schwartz, R., and Doughty, A. M.: Glacier retreat in New Zealand during the Younger Dryas stadial, Nature, 467, 194-197, https://doi.org/10.1038/nature09313, 2010.

Karancz, S., de Nooijer, L. J., van der Wagt, B., van der Meer, M. T. J., Misra, S., Hennekam, R., Erdem, Z., Lattaud, J., Haghipour, N., Schouten, S., and Reichart, G.-J.: Dataset belonging to "Contrasts in the marine inorganic carbon chemistry of the Benguela Upwelling System since the Last Glacial Maximum" (V3), NIOZ [dataset], https://doi.org/10.25850/nioz/7b.b.lh, 2024.

Key, R. M., Olsen, A., van Heuven, S., Lauvset, S. K., Velo, A., Lin, X., Schirnick, C., Kozyr, A., Tanhua, T., Hoppema, M., Jutterström, S., Steinfeldt, R., Jeansson, E., Ishii, M., Perez, F. F., and Suzuki, T.: Global Ocean Data Analysis Project, Version 2 (GLODAPv2), https://doi.org/10.3334/CDIAC/OTG.NDP093_GLODAPv2, 2015.

Kirst, G. J., Schneider, R. R., Müller, P. J., von Storch, I., and Wefer, G.: Late Quaternary temperature variability in the Benguela Current System derived from alkenones, Quatern. Res., 52, 92-103, https://doi.org/10.1006/qres.1999.2040, 1999.

Klaas, C. and Archer, D. E.: Association of sinking organic matter with various types of mineral ballast in the deep sea: Implications for the rain ratio, Global Biogeochem. Cycles, 16, 63-61-63-14, https://doi.org/10.1029/2001GB001765, 2002.

Klochko, K., Kaufman, A. J., Yao, W., Byrne, R. H., and Tossell, J. A.: Experimental measurement of boron isotope fractionation in seawater, Earth. Planet. Sci. Lett., 248, 276-285, https://doi.org/10.1016/j.epsl.2006.05.034, 2006.

Knorr, G. and Lohmann, G.: Southern Ocean origin for the resumption of Atlantic thermohaline circulation during deglaciation, Nature, 424, 532-536, https://doi.org/10.1038/nature01855, 2003.

Kohfeld, K. E., Quéré, C. L., Harrison, S. P., and Anderson, R. F.: Role of marine biology in glacial-interglacial CO_2 cycles, Science, 308, 74-78, https://doi.org/10.1126/science.1105375, 2005.

Kozdon, R., Kelly, D. C., Kitajima, K., Strickland, A., Fournelle, J. H., and Valley, J. W.: In situ $\delta^{18}O$ and Mg/Ca analyses of diagenetic and planktic foraminiferal calcite preserved in a deep-sea record of the Paleocene-Eocene thermal maximum, Paleoceanography, 28, 517-528, https://doi.org/10.1002/palo.20048, 2013.

Kroopnick, P.: The distribution of ^{13}C in the Atlantic Ocean, Earth. Planet. Sci. Lett., 49, 469-484, https://doi.org/10.1016/0012-821X(80)90088-6, 1980.

Kroopnick, P. M.: The distribution of ^{13}C of ΣCO_2 in the world oceans, Deep Sea Research Part A. Oceanographic Research Papers, 32, 57-84, https://doi.org/10.1016/0198-0149(85)90017-2, 1985.

Kwon, E. Y., Primeau, F., and Sarmiento, J. L.: The impact of remineralization depth on the air–sea carbon balance, Nat. Geosci., 2, 630-635, https://doi.org/10.1038/ngeo612, 2009.

Lamy, F., Kaiser, J., Arz, H. W., Hebbeln, D., Ninnemann, U., Timm, O., Timmermann, A., and Toggweiler, J. R.: Modulation of the bipolar seesaw in the Southeast Pacific during Termination 1, Earth. Planet. Sci. Lett., 259, 400-413, https://doi.org/10.1016/j.epsl.2007.04.040, 2007.

Laruelle, G. G., Lauerwald, R., Pfeil, B., and Regnier, P.: Regionalized global budget of the CO_2 exchange at the air-water interface in continental shelf seas, Global Biogeochem. Cycles, 28, 1199-1214, https://doi.org/10.1002/2014GB004832, 2014.

Formatted: Font: (Default) Times New Roman

Lauvset, S. K., Lange, N., Tanhua, T., Bittig, H. C., Olsen, A., Kozyr, A., Álvarez, M., Azetsu-Scott, K., Brown, P. J., Carter, B. R., Cotrim da Cunha, L., Hoppema, M., Humphreys, M. P., Ishii, M., Jeansson, E., Murata, A., Müller, J. D., Perez, F. F., Schirnick, C., Steinfeldt, R., Suzuki, T., Ulfsbo, A., Velo, A., Woosley, R. J., and Key, R.: The annual update GLODAPv2.2023: the global interior ocean biogeochemical data product, Earth Syst. Sci. Data Discuss., 2024, 1-32, https://doi.org/10.5194/essd-2023-468, 2024.

Laws, E. A., Falkowski, P. G., Smith Jr, W. O., Ducklow, H., and McCarthy, J. J.: Temperature effects on export production in the open ocean, Global Biogeochem. Cycles, 14, 1231-1246, https://doi.org/10.1029/1999GB001229, 2000.

Laws, E. A., Popp, B. N., Bidigare, R. R., Kennicutt, M. C., and Macko, S. A.: Dependence of phytoplankton carbon isotopic composition on growth rate and $[CO_2]_{aq}$: Theoretical considerations and experimental results, Geochim. Cosmochim. Acta, 59, 1131-1138, https://doi.org/10.1016/0016-7037(95)00030-4, 1995.

Lea, D. and Boyle, E.: Barium content of benthic foraminifera controlled by bottom-water composition, Nature, 338, 751-753, https://doi.org/10.1038/338751a0, 1989.

Lea, D. W. and Boyle, E. A.: A 210,000-year record of barium variability in the deep northwest Atlantic Ocean, Nature, 347, 269-272, https://doi.org/10.1038/347269a0, 1990a.

Lea, D. W. and Boyle, E. A.: Foraminiferal reconstruction of barium distributions in water masses of the glacial oceans, Paleoceanography, 5, 719-742, https://doi.org/10.1029/PA005i005p00719, 1990b.

Lea, D. W. and Boyle, E. A.: Barium in planktonic foraminifera, Geochim. Cosmochim. Acta, 55, 3321-3331, https://doi.org/10.1016/0016-7037(91)90491-M, 1991.

Lea, D. W. and Spero, H. J.: Assessing the reliability of paleochemical tracers: Barium uptake in the shells of planktonic foraminifera, Paleoceanography, 9, 445-452, https://doi.org/10.1029/94PA00151, 1994.

Leduc, G., Schneider, R., Kim, J. H., and Lohmann, G.: Holocene and Eemian sea surface temperature trends as revealed by alkenone and Mg/Ca paleothermometry, Quat. Sci. Rev., 29, 989-1004, https://doi.org/10.1016/j.quascirev.2010.01.004, 2010.

Lessa, D., Morard, R., Jonkers, L., Venancio, I. M., Reuter, R., Baumeister, A., Albuquerque, A. L., and Kucera, M.: Distribution of planktonic foraminifera in the subtropical South Atlantic: depth hierarchy of controlling factors, Biogeosciences, 17, 4313-4342, https://doi.org/10.5194/bg-17-4313-2020, 2020.

Li, L., Liu, Z., Zhu, C., He, C., and Otto-Bliesner, B.: Shallowing Glacial Antarctic Intermediate Water by changes in sea ice and hydrological cycle, Geophys. Res. Lett., 48, e2021GL094317, https://doi.org/10.1029/2021GL094317, 2021.

Little, M., Schneider, R., Kroon, D., Price, B., Bickert, T., and Wefer, G.: Rapid palaeoceanographic changes in the Benguela Upwelling System for the last 160,000 years as indicated by abundances of planktonic foraminifera, Palaeogeogr., Palaeoclimatol., Palaeoecol., 130, 135-161, https://doi.org/10.1016/S0031-0182(96)00136-8, 1997.

Ljung, K., Björck, S., Renssen, H., and Hammarlund, D.: South Atlantic island record reveals a South Atlantic response to the 8.2 kyr event, Clim. Past, 4, 35-45, https://doi.org/10.5194/cp-4-35-2008, 2008.

Lloyd, N. S., Sadekov, A. Y., and Misra, S.: Application of 10^{13} ohm Faraday cup current amplifiers for boron isotopic analyses by solution mode and laser ablation multicollector inductively coupled plasma mass spectrometry, Rapid Commun. Mass Spectrom., 32, 9-18, https://doi.org/10.1002/rcm.8009, 2018.

Formatted: Font: (Default) Times New Roman

Longhurst, A. R. and Glen Harrison, W.: The biological pump: Profiles of plankton production and consumption in the upper ocean, Prog. Oceanogr., 22, 47-123, https://doi.org/10.1016/0079-6611(89)90010-4, 1989.

Lutjeharms, J. and Meeuwis, J.: The extent and variability of South-East Atlantic upwelling, S. Afr. J. Mar. Sci., 5, 51-62, https://doi.org/10.2989/025776187784522621, 1987.

Lutjeharms, J. and Valentine, H.: Water types and volumetric considerations of the South-East Atlantic upwelling regime, S. Afr. J. Mar. Sci., 5, 63-71, https://doi.org/10.2989/025776187784522487, 1987.

Lutjeharms, J. R. E. and Stockton, P. L.: Kinematics of the upwelling front off southern Africa, S. Afr. J. Mar. Sci., 5, 35-49, https://doi.org/10.2989/025776187784522612, 1987.

Lynch-Stieglitz, J., Stocker, T. F., Broecker, W. S., and Fairbanks, R. G.: The influence of air-sea exchange on the isotopic composition of oceanic carbon: Observations and modeling, Global Biogeochem. Cycles, 9, 653-665, https://doi.org/10.1029/95GB02574, 1995.

Martin, J. H.: Glacial-interglacial CO_2 change: The iron hypothesis, Paleoceanography, 5, 1-13, https://doi.org/10.1029/PA005i001p00001, 1990.

Martin, P. A. and Lea, D. W.: Comparison of water mass changes in the deep tropical Atlantic derived from Cd/Ca and carbon isotope records: Implications for changing Ba composition of Deep Atlantic Water Masses, Paleoceanography, 13, 572-585, https://doi.org/10.1029/98PA02670, 1998.

Martínez-García, A., Sigman, D. M., Ren, H., Anderson, R. F., Straub, M., Hodell, D. A., Jaccard, S. L., Eglinton, T. I., and Haug, G. H.: Iron fertilization of the Subantarctic Ocean during the Last Ice Age, Science, 343, 1347-1350, https://doi.org/10.1126/science.1246848, 2014.

Mashiotta, T. A., Lea, D. W., and Spero, H. J.: Glacial–interglacial changes in Subantarctic sea surface temperature and δ^{18}O-water using foraminiferal Mg, Earth. Planet. Sci. Lett., 170, 417-432, https://doi.org/10.1016/S0012-821X(99)00116-8, 1999.

Matero, I. S. O., Gregoire, L. J., Ivanovic, R. F., Tindall, J. C., and Haywood, A. M.: The 8.2 ka cooling event caused by Laurentide ice saddle collapse, Earth. Planet. Sci. Lett., 473, 205-214, https://doi.org/10.1016/j.epsl.2017.06.011, 2017.

McManus, J. F., Francois, R., Gherardi, J. M., Keigwin, L. D., and Brown-Leger, S.: Collapse and rapid resumption of Atlantic meridional circulation linked to deglacial climate changes, Nature, 428, 834-837, https://doi.org/10.1038/nature02494, 2004.

McManus, J. F., Bond, G. C., Broecker, W. S., Johnsen, S., Labeyrie, L., and Higgins, S.: High-resolution climate records from the North Atlantic during the last interglacial, Nature, 371, 326-329, https://doi.org/10.1038/371326a0, 1994.

Mekik, F., François, R., and Soon, M.: A novel approach to dissolution correction of Mg/Ca–based paleothermometry in the tropical Pacific, Paleoceanography, 22, https://doi.org/10.1029/2007PA001504, 2007.

Mezger, E., De Nooijer, L., Boer, W., Brummer, G., and Reichart, G.: Salinity controls on Na incorporation in Red Sea planktonic foraminifera, Paleoceanography, 31, 1562-1582, https://doi.org/10.1002/2016PA003052, 2016.

Misra, S., Owen, R., Kerr, J., Greaves, M., and Elderfield, H.: Determination of δ^{11}B by HR-ICP-MS from mass limited samples: Application to natural carbonates and water samples, Geochim. Cosmochim. Acta, 140, 531-552, https://doi.org/10.1016/j.gca.2014.05.047, 2014.

Mollenhauer, G., Schneider, R. R., Müller, P. J., Spieß, V., and Wefer, G.: Glacial/interglacial variablity in the Benguela upwelling system: Spatial distribution and budgets of organic carbon accumulation, Global Biogeochem. Cycles, 16, 81-81-81-15, https://doi.org/10.1029/2001GB001488, 2002.

Formatted: Font: (Default) Times New Roman

Mollenhauer, G., Eglinton, T. I., Ohkouchi, N., Schneider, R. R., Müller, P. J., Grootes, P. M., and Rullkötter, J.: Asynchronous alkenone and foraminifera records from the Benguela Upwelling System, Geochim. Cosmochim. Acta, 67, 2157-2171, https://doi.org/10.1016/s0016-7037(03)00168-6, 2003.

Mook, W. G., Bommerson, J. C., and Staverman, W. H.: Carbon isotope fractionation between dissolved bicarbonate and gaseous carbon dioxide, Earth. Planet. Sci. Lett., 22, 169-176, https://doi.org/10.1016/0012-821X(74)90078-8, 1974.

Muller-Karger, F. E., Varela, R., Thunell, R., Luerssen, R., Hu, C., and Walsh, J. J.: The importance of continental margins in the global carbon cycle, Geophys. Res. Lett., 32, https://doi.org/10.1029/2004GL021346, 2005.

Muratli, J. M., Chase, Z., Mix, A. C., and McManus, J.: Increased glacial-age ventilation of the Chilean margin by Antarctic Intermediate Water, Nat. Geosci., 3, 23-26, https://doi.org/10.1038/ngeo715, 2010.

Ni, S., Quintana Krupinski, N. B., Groeneveld, J., Persson, P., Somogyi, A., Brinkmann, I., Knudsen, K. L., Seidenkrantz, M. S., and Filipsson, H. L.: Early diagenesis of foraminiferal calcite under anoxic conditions: A case study from the Landsort Deep, Baltic Sea (IODP Site M0063), Chem. Geol., 558, 119871, https://doi.org/10.1016/j.chemgeo.2020.119871, 2020.

North Greenland Ice Core Project members: High-resolution record of Northern Hemisphere climate extending into the last interglacial period, Nature, 431, 147-151, https://doi.org/10.1038/nature02805, 2004.

Oberhänsli, H.: Upwelling signals at the northeastern Walvis Ridge during the past 500,000 years, Paleoceanography, 6, 53-71, https://doi.org/10.1029/90PA02106, 1991.

Okai, T., Suzuki, A., Terashima, S., Inoue, M., Nohara, M., Kawahata, H., and Imai, N.: Collaborative analysis of GSJ/AIST geochemical reference materials JCp-1 (Coral) and JCt-1 (Giant Clam), Geochem, 38, 281-286, 2004.

Olsen, A., Key, R. M., van Heuven, S., Lauvset, S. K., Velo, A., Lin, X., Schirnick, C., Kozyr, A., Tanhua, T., Hoppema, M., Jutterström, S., Steinfeldt, R., Jeansson, E., Ishii, M., Pérez, F. F., and Suzuki, T.: The Global Ocean Data Analysis Project version 2 (GLODAPv2) – an internally consistent data product for the world ocean, Earth Syst. Sci. Data, 8, 297-323, https://doi.org/10.5194/essd-8-297-2016, 2016.

Oppo, D. W. and Fairbanks, R. G.: Carbon isotope composition of tropical surface water during the past 22,000 years, Paleoceanography, 4, 333-351, https://doi.org/10.1029/PA004i004p00333, 1989.

Oppo, D. W. and Rosenthal, Y.: Cd/Ca changes in a Deep Cape Basin Core over the past 730,000 years: Response of circumpolar deepwater variability to northern hemisphere ice sheet melting?, Paleoceanography, 9, 661-675, https://doi.org/10.1029/93PA02199, 1994.

Pagani, M.: Biomarker-based inferences of past climate: The alkenone pCO_2 Proxy, in: Treatise on Geochemistry, 361-378, https://doi.org/10.1016/b978-0-08-095975-7.01027-5, 2014.

Pagani, M., Arthur, M. A., and Freeman, K. H.: Miocene evolution of atmospheric carbon dioxide, Paleoceanography, 14, 273-292, https://doi.org/10.1029/1999PA900006, 1999.

Pagani, M., Freeman, K. H., Ohkouchi, N., and Caldeira, K.: Comparison of water column [CO_{2aq}] with sedimentary alkenone-based estimates: A test of the alkenone-CO_2 proxy, Paleoceanography, 17, 21-21-21-12, https://doi.org/10.1029/2002pa000756, 2002.

Pagani, M., Liu, Z., LaRiviere, J., and Ravelo, A. C.: High Earth-system climate sensitivity determined from Pliocene carbon dioxide concentrations, Nat. Geosci., 3, 27-30, https://doi.org/10.1038/ngeo724, 2010.

Pagani, M., Zachos, J. C., Freeman, K. H., Tipple, B., and Bohaty, S.: Marked decline in atmospheric carbon dioxide concentrations during the Paleogene, Science, 309, 600-603, https://doi.org/10.1126/science.1110063, 2005.

Formatted: Font: (Default) Times New Roman

Pagani, M., Huber, M., Liu, Z., Bohaty, S. M., Henderiks, J., Sijp, W., Krishnan, S., and DeConto, R. M.: The role of carbon dioxide during the onset of Antarctic Glaciation, Science, 334, 1261-1264, https://doi.org/10.1126/science.1203909, 2011.

Pahnke, K., Goldstein, S. L., and Hemming, S. R.: Abrupt changes in Antarctic Intermediate Water circulation over the past 25,000 years, Nat. Geosci., 1, 870-874, https://doi.org/10.1038/ngeo360, 2008.

Palmer, M. and Pearson, P. N.: A 23,000-year record of surface water pH and PCO_2 in the western equatorial Pacific Ocean, Science, 300, 480-482, https://doi.org/10.1126/science.108079, 2003.

Palmer, M. R., Brummer, G. J., Cooper, M. J., Elderfield, H., Greaves, M. J., Reichart, G. J., Schouten, S., and Yu, J. M.: Multi-proxy reconstruction of surface water pCO_2 in the northern Arabian Sea since 29 ka, Earth. Planet. Sci. Lett., 295, 49-57, https://doi.org/10.1016/j.epsl.2010.03.023, 2010.

Panieri, G., Lepland, A., Whitehouse, M. J., Wirth, R., Raanes, M. P., James, R. H., Graves, C. A., Crémière, A., and Schneider, A.: Diagenetic Mg-calcite overgrowths on foraminiferal tests in the vicinity of methane seeps, Earth. Planet. Sci. Lett., 458, 203-212, https://doi.org/10.1016/j.epsl.2016.10.024, 2017.

Panmei, C., Divakar Naidu, P., and Mohtadi, M.: Bay of Bengal exhibits warming trend during the Younger Dryas: Implications of AMOC, Geochem. Geophys. Geosyst., 18, 4317-4325, https://doi.org/10.1002/2017GC007075, 2017.

Parekh, P., Dutkiewicz, S., Follows, M. J., and Ito, T.: Atmospheric carbon dioxide in a less dusty world, Geophys. Res. Lett., 33, https://doi.org/10.1029/2005GL025098, 2006.

Partridge, T. C., Scott, L., and Hamilton, J. E.: Synthetic reconstructions of southern African environments during the Last Glacial Maximum (21–18 kyr) and the Holocene Altithermal (8–6 kyr), Quat. Int., 57-58, 207-214, https://doi.org/10.1016/S1040-6182(98)00061-5, 1999.

Pedro, J. B., Bostock, H. C., Bitz, C. M., He, F., Vandergoes, M. J., Steig, E. J., Chase, B. M., Krause, C. E., Rasmussen, S. O., Markle, B. R., and Cortese, G.: The spatial extent and dynamics of the Antarctic Cold Reversal, Nat. Geosci., 9, 51-55, https://doi.org/10.1038/ngeo2580, 2016.

Peeters, F. J., Acheson, R., Brummer, G.-J. A., De Ruijter, W. P., Schneider, R. R., Ganssen, G. M., Ufkes, E., and Kroon, D.: Vigorous exchange between the Indian and Atlantic oceans at the end of the past five glacial periods, Nature, 430, 661-665, https://doi.org/10.1038/nature02785, 2004.

Peterson, R. G. and Stramma, L.: Upper-level circulation in the South Atlantic Ocean, Prog. Oceanogr., 26, 1-73, https://doi.org/10.1016/0079-6611(91)90006-8, 1991.

Pether, J.: Molluscan evidence for enhanced deglacial advection of Agulhas water in the Benguela current, off southwestern Africa, Palaeogeogr., Palaeoclimatol., Palaeoecol., 111, 99-117, https://doi.org/10.1016/0031-0182(94)90350-6, 1994.

Petit, J. R., Jouzel, J., Raynaud, D., Barkov, N. I., Barnola, J. M., Basile, I., Bender, M., Chappellaz, J., Davis, M., Delaygue, G., Delmotte, M., Kotlyakov, V. M., Legrand, M., Lipenkov, V. Y., Lorius, C., PÉpin, L., Ritz, C., Saltzman, E., and Stievenard, M.: Climate and atmospheric history of the past 420,000 years from the Vostok ice core, Antarctica, Nature, 399, 429-436, https://doi.org/10.1038/20859, 1999.

Popp, B. N., Laws, E. A., Bidigare, R. R., Dore, J. E., Hanson, K. L., and Wakeham, S. G.: Effect of phytoplankton cell geometry on carbon isotopic fractionation, Geochim. Cosmochim. Acta, 62, 69-77, https://doi.org/10.1016/S0016-7037(97)00333-5, 1998.

Pöppelmeier, F., Jeltsch-Thömmes, A., Lippold, J., Joos, F., and Stocker, T. F.: Multi-proxy constraints on Atlantic circulation dynamics since the last ice age, Nat. Geosci., 16, 349-356, https://doi.org/10.1038/s41561-023-01140-3, 2023.

Formatted: Font: (Default) Times New Roman

Prahl, F. G. and Wakeham, S. G.: Calibration of unsaturation patterns in long-chain ketone compositions for palaeotemperature assessment, Nature, 330, 367-369, https://doi.org/10.1038/330367a0, 1987.

Rae, J. W. B., Zhang, Y. G., Liu, X., Foster, G. L., Stoll, H. M., and Whiteford, R. D. M.: Atmospheric CO_2 over the Past 66 Million Years from Marine Archives, Annu. Rev. Earth Planet. Sci., 49, 609-641, https://doi.org/10.1146/annurev-earth-082420-063026, 2021.

Rahmstorf, S.: Ocean circulation and climate during the past 120,000 years, Nature, 419, 207-214, https://doi.org/10.1038/nature01090, 2002.

Raitzsch, M., Bijma, J., Benthien, A., Richter, K.-U., Steinhoefel, G., and Kučera, M.: Boron isotope-based seasonal paleo-pH reconstruction for the Southeast Atlantic – A multispecies approach using habitat preference of planktonic foraminifera, Earth. Planet. Sci. Lett., 487, 138-150, https://doi.org/10.1016/j.epsl.2018.02.002, 2018.

Rau, A. J., Rogers, J., Lutjeharms, J. R. E., Giraudeau, J., Lee-Thorp, J. A., Chen, M. T., and Waelbroeck, C.: A 450-kyr record of hydrological conditions on the western Agulhas Bank Slope, south of Africa, Mar. Geol., 180, 183-201, https://doi.org/10.1016/S0025-3227(01)00213-4, 2002.

Rau, G. H., Riebesell, U., and Wolf-Gladrow, D.: A model of photosynthetic ^{13}C fractionation by marine phytoplankton based on diffusive molecular CO_2 uptake, Mar. Ecol. Prog. Ser., 133, 275-285, https://doi.org/10.3354/meps133275, 1996.

Rebotim, A., Voelker, A. H. L., Jonkers, L., Waniek, J. J., Meggers, H., Schiebel, R., Fraile, I., Schulz, M., and Kucera, M.: Factors controlling the depth habitat of planktonic foraminifera in the subtropical eastern North Atlantic, Biogeosciences, 14, 827-859, https://doi.org/10.5194/bg-14-827-2017, 2017.

Redfield, A. C.: The biological control of chemical factors in the environment, American Scientist, 46, 230A-221, 1958.

Regenberg, M., Nürnberg, D., Steph, S., Groeneveld, J., Garbe-Schönberg, D., Tiedemann, R., and Dullo, W. C.: Assessing the effect of dissolution on planktonic foraminiferal Mg/Ca ratios: Evidence from Caribbean core tops, Geochem. Geophys. Geosyst., 7, https://doi.org/10.1029/2005GC001019, 2006.

Reinfelder, J. R.: Carbon concentrating mechanisms in eukaryotic marine phytoplankton, Ann. Rev. Mar. Sci., 3, 291-315, https://doi.org/10.1146/annurev-marine-120709-142720, 2011.

Riebesell, U., Revill, A. T., Holdsworth, D. G., and Volkman, J. K.: The effects of varying CO_2 concentration on lipid composition and carbon isotope fractionation in *Emiliania huxleyi*, Geochim. Cosmochim. Acta, 64, 4179-4192, https://doi.org/10.1016/S0016-7037(00)00474-9, 2000.

Romanek, C. S., Grossman, E. L., and Morse, J. W.: Carbon isotopic fractionation in synthetic aragonite and calcite: Effects of temperature and precipitation rate, Geochim. Cosmochim. Acta, 56, 419-430, https://doi.org/10.1016/0016-7037(92)90142-6, 1992.

Ronge, T. A., Steph, S., Tiedemann, R., Prange, M., Merkel, U., Nürnberg, D., and Kuhn, G.: Pushing the boundaries: Glacial/interglacial variability of intermediate and deep waters in the southwest Pacific over the last 350,000 years, Paleoceanography, 30, 23-38, https://doi.org/10.1002/2014PA002727, 2015.

Roobaert, A., Laruelle, G. G., Landschützer, P., Gruber, N., Chou, L., and Regnier, P.: The spatiotemporal dynamics of the sources and sinks of CO_2 in the global coastal ocean, Global Biogeochem. Cycles, 33, 1693-1714, https://doi.org/10.1029/2019GB006239, 2019.

Rühlemann, C., Mulitza, S., Müller, P. J., Wefer, G., and Zahn, R.: Warming of the tropical Atlantic Ocean and slowdown of thermohaline circulation during the last deglaciation, Nature, 402, 511-514, https://doi.org/10.1038/990069, 1999.

Formatted: Font: (Default) Times New Roman

Salt, L. A., van Heuven, S. M. A. C., Claus, M. E., Jones, E. M., and de Baar, H. J. W.: Rapid acidification of mode and intermediate waters in the southwestern Atlantic Ocean, Biogeosciences, 12, 1387-1401, https://doi.org/10.5194/bg-12-1387-2015, 2015.

Santana-Casiano, J. M., González-Dávila, M., and Ucha, I. R.: Carbon dioxide fluxes in the Benguela upwelling system during winter and spring: A comparison between 2005 and 2006, Deep Sea Research Part II: Topical Studies in Oceanography, 56, 533-541, https://doi.org/10.1016/j.dsr2.2008.12.010, 2009.

Sarnthein, M., Winn, K., Jung, S. J. A., Duplessy, J.-C., Labeyrie, L., Erlenkeuser, H., and Ganssen, G.: Changes in East Atlantic Deepwater Circulation over the last 30,000 years: Eight time slice reconstructions, Paleoceanography, 9, 209-267, https://doi.org/10.1029/93PA03301, 1994.

Schlitzer, R.: eWOCE-Electronic Atlas of WOCE Data, WOCE Global Data, Version 2.0 CD-ROM, WOCE Intern. Project Office, WOCE Report No. 171/00, Southampton, UK, 2000.

Schmittner, A., Gruber, N., Mix, A. C., Key, R. M., Tagliabue, A., and Westberry, T. K.: Biology and air-sea gas exchange controls on the distribution of carbon isotope ratios ($\delta^{13}C$) in the ocean, Biogeosciences, 10, 5793-5816, https://doi.org/10.5194/bg-10-5793-2013, 2013.

Schouten, S., Klein Breteler, W. C. M., Blokker, P., Schogt, N., Rijpstra, W. I. C., Grice, K., Baas, M., and Sinninghe Damsté, J. S.: Biosynthetic effects on the stable carbon isotopic compositions of algal lipids: implications for deciphering the carbon isotopic biomarker record, Geochim. Cosmochim. Acta, 62, 1397-1406, https://doi.org/10.1016/S0016-7037(98)00076-3, 1998.

Scussolini, P. and Peeters, F. J.: A record of the last 460 thousand years of upper ocean stratification from the central Walvis Ridge, South Atlantic, Paleoceanography, 28, 426-439, https://doi.org/10.1002/palo.20041, 2013.

Seki, O., Foster, G. L., Schmidt, D. N., Mackensen, A., Kawamura, K., and Pancost, R. D.: Alkenone and boron-based Pliocene pCO_2 records, Earth. Planet. Sci. Lett., 292, 201-211, https://doi.org/10.1016/j.epsl.2010.01.037, 2010.

Sexton, P. F., Wilson, P. A., and Pearson, P. N.: Microstructural and geochemical perspectives on planktic foraminiferal preservation: "Glassy" versus "Frosty", Geochem. Geophys. Geosyst., 7, n/a-n/a, https://doi.org/10.1029/2006gc001291, 2006.

Shannon, L. and Nelson, G.: The Benguela: large scale features and processes and system variability, in: The south atlantic, Springer, Berlin, Heidelberg, 163-210, https://doi.org/10.1007/978-3-642-80353-6_9, 1996.

Shannon, L. V. and O'Toole, M.: Sustainability of the Benguela: ex Africa semper aliquid novi, in: Large Marine Ecosystems of the World: Trends in Exploitation, Protection and Research, edited by: Hempel, G., and Sherman, K., Elsevier B.V., Amsterdam, 227-253, 2003.

Shi, N., Dupont, L. M., Beug, H.-J., and Schneider, R.: Vegetation and climate changes during the last 21 000 years in S.W. Africa based on a marine pollen record, Veg. Hist. Archaeobot., 7, 127-140, https://doi.org/10.1007/BF01374001, 1998.

Shillington, F.: The Benguela upwelling system off southwestern Africa, The sea, 11, 583-604, 1998.

Spero, H. J.: Do planktic foraminifera accurately record shifts in the carbon isotopic composition of seawater ΣCO_2?, Mar. Micropaleontol., 19, 275-285, https://doi.org/10.1016/0377-8398(92)90033-G, 1992.

Spero, H. J. and Lea, D. W.: Intraspecific stable isotope variability in the planktic foraminifera *Globigerinoides sacculifer*: Results from laboratory experiments, Mar. Micropaleontol., 22, 221-234, https://doi.org/10.1016/0377-8398(93)90045-Y, 1993.

Spero, H. J. and Lea, D. W.: Experimental determination of stable isotope variability in *Globigerina bulloides*: implications for paleoceanographic reconstructions, Mar. Micropaleontol., 28, 231-246, https://doi.org/10.1016/0377-8398(96)00003-5, 1996.

Formatted: Font: (Default) Times New Roman

Spero, H. J., Bijma, J., Lea, D. W., and Bemis, B. E.: Effect of seawater carbonate concentration on foraminiferal carbon and oxygen isotopes, Nature, 390, 497-500, https://doi.org/10.1038/37333, 1997.

Stainbank, S., Spezzaferri, S., De Boever, E., Bouvier, A.-S., Chilcott, C., De Leau, E. S., Foubert, A., Kunkelova, T., Pichevin, L., Raddatz, J., Rüggeberg, A., Wright, J. D., Yu, S. M., Zhang, M., and Kroon, D.: Assessing the impact of diagenesis on foraminiferal geochemistry from a low latitude, shallow-water drift deposit, Earth. Planet. Sci. Lett., 545, 116390, https://doi.org/10.1016/j.epsl.2020.116390, 2020.

Stephens, B. B. and Keeling, R. F.: The influence of Antarctic sea ice on glacial–interglacial CO_2 variations, Nature, 404, 171-174, https://doi.org/10.1038/35004556, 2000.

Stocker, T. F.: The Seesaw Effect, Science, 282, 61-62, https://doi.org/10.1126/science.282.5386.61, 1998.

Stoll, H. M., Guitian, J., Hernandez-Almeida, I., Mejia, L. M., Phelps, S., Polissar, P., Rosenthal, Y., Zhang, H., and Ziveri, P.: Upregulation of phytoplankton carbon concentrating mechanisms during low CO_2 glacial periods and implications for the phytoplankton pCO_2 proxy, Quat. Sci. Rev., 208, 1-20, https://doi.org/10.1016/j.quascirev.2019.01.012, 2019.

Stramma, L. and England, M.: On the water masses and mean circulation of the South Atlantic Ocean, J. Geophys. Res. Oceans, 104, 20863-20883, https://doi.org/10.1029/1999JC900139, 1999.

Stuut, J.-B. W., Prins, M. A., Schneider, R. R., Weltje, G. J., Jansen, J. H. F., and Postma, G.: A 300-kyr record of aridity and wind strength in southwestern Africa: inferences from grain-size distributions of sediments on Walvis Ridge, SE Atlantic, Mar. Geol., 180, 221-233, https://doi.org/10.1016/S0025-3227(01)00215-8, 2002.

Suggate, R. P. and Almond, P. C.: The Last Glacial Maximum (LGM) in western South Island, New Zealand: implications for the global LGM and MIS 2, Quat. Sci. Rev., 24, 1923-1940, https://doi.org/10.1016/j.quascirev.2004.11.007, 2005.

Synal, H.-A., Stocker, M., and Suter, M.: MICADAS: A new compact radiocarbon AMS system, Nuclear Instruments and Methods in Physics Research Section B: Beam Interactions with Materials and Atoms, 259, 7-13, https://doi.org/10.1016/j.nimb.2007.01.138, 2007.

Tapia, R., Ho, S. L., Wang, H. Y., Groeneveld, J., and Mohtadi, M.: Contrasting vertical distributions of recent planktic foraminifera off Indonesia during the southeast monsoon: implications for paleoceanographic reconstructions, Biogeosciences, 19, 3185-3208, https://doi.org/10.5194/bg-19-3185-2022, 2022.

Thomas, E. and Shackleton, N. J.: The Paleocene-Eocene benthic foraminiferal extinction and stable isotope anomalies, Geological Society, London, Special Publications, 101, 401-441, https://doi.org/10.1144/GSL.SP.1996.101.01.20, 1996.

Tian, H.-A., van Manen, M., Bunnell, Z. B., Jung, J., Lee, S. H., Kim, T.-W., Reichart, G.-J., Conway, T. M., and Middag, R.: Biogeochemistry of iron in coastal Antarctica: isotopic insights for external sources and biological uptake in the Amundsen Sea polynyas, Geochim. Cosmochim. Acta, 363, 51-67, https://doi.org/10.1016/j.gca.2023.10.029, 2023.

Turi, G., Lachkar, Z., and Gruber, N.: Spatiotemporal variability and drivers of pCO_2 and air–sea CO_2 fluxes in the California Current System: an eddy-resolving modeling study, Biogeosciences, 11, 671-690, https://doi.org/10.5194/bg-11-671-2014, 2014.

Turner, J. T.: Zooplankton fecal pellets, marine snow, phytodetritus and the ocean's biological pump, Prog. Oceanogr., 130, 205-248, https://doi.org/10.1016/j.pocean.2014.08.005, 2015.

Van Dijk, I., de Nooijer, L. J., Wolthers, M., and Reichart, G.-J.: Impacts of pH and $[CO_3^{2-}]$ on the incorporation of Zn in foraminiferal calcite, Geochim. Cosmochim. Acta, 197, 263-277, https://doi.org/10.1016/j.gca.2016.10.031, 2017.

Formatted: Font: (Default) Times New Roman

van Dongen, B. E., Schouten, S., and Damsté, J. S. S.: Carbon isotope variability in monosaccharides and lipids of aquatic algae and terrestrial plants, Mar. Ecol. Prog. Ser., 232, 83-92, https://doi.org/10.3354/meps232083, 2002.

Vandergoes, M. J., Dieffenbacher-Krall, A. C., Newnham, R. M., Denton, G. H., and Blaauw, M.: Cooling and changing seasonality in the Southern Alps, New Zealand during the Antarctic Cold Reversal, Quat. Sci. Rev., 27, 589-601, https://doi.org/10.1016/j.quascirev.2007.11.015, 2008.

Volk, T. and Hoffert, M. I.: Ocean carbon pumps: Analysis of relative strengths and efficiencies in ocean-driven atmospheric CO_2 changes, in: The carbon cycle and atmospheric CO_2: Natural variations archean to present, Geophysical Monograph Series, 99-110, https://doi.org/10.1029/GM032p0099, 1985.

Wacker, L., Güttler, D., Goll, J., Hurni, J. P., Synal, H. A., and Walti, N.: Radiocarbon dating to a single year by means of rapid atmospheric ^{14}C changes, Radiocarbon, 56, 573-579, https://doi.org/10.2458/56.17634, 2014.

Wacker, L., Fahrni, S. M., Hajdas, I., Molnar, M., Synal, H. A., Szidat, S., and Zhang, Y. L.: A versatile gas interface for routine radiocarbon analysis with a gas ion source, Nuclear Instruments and Methods in Physics Research Section B: Beam Interactions with Materials and Atoms, 294, 315-319, https://doi.org/10.1016/j.nimb.2012.02.009, 2013.

Waelbroeck, C., Labeyrie, L., Michel, E., Duplessy, J. C., McManus, J. F., Lambeck, K., Balbon, E., and Labracherie, M.: Sea-level and deep water temperature changes derived from benthic foraminifera isotopic records, Quat. Sci. Rev., 21, 295-305, https://doi.org/10.1016/S0277-3791(01)00101-9, 2002.

Wang, B.-S., You, C.-F., Huang, K.-F., Wu, S.-F., Aggarwal, S. K., Chung, C.-H., and Lin, P.-Y.: Direct separation of boron from Na- and Ca-rich matrices by sublimation for stable isotope measurement by MC-ICP-MS, Talanta, 82, 1378-1384, https://doi.org/10.1016/j.talanta.2010.07.010, 2010.

Wang, Y. V., Leduc, G., Regenberg, M., Andersen, N., Larsen, T., Blanz, T., and Schneider, R. R.: Northern and southern hemisphere controls on seasonal sea surface temperatures in the Indian Ocean during the last deglaciation, Paleoceanography, 28, 619-632, https://doi.org/10.1002/palo.20053, 2013.

Wefer, G. a., Berger, W. H., Bickert, T., Donner, B., Fischer, G., von Mücke, S. K., Meinecke, G., Müller, P., Mulitza, S., and Niebler, H.-S.: Late Quaternary surface circulation of the South Atlantic: The stable isotope record and implications for heat transport and productivity, in: The South Atlantic, Springer, Berlin, Heidelberg, 461-502, https://doi.org/10.1007/978-3-642-80353-6_25, 1996.

Weltje, G. J. and Tjallingii, R.: Calibration of XRF core scanners for quantitative geochemical logging of sediment cores: Theory and application, Earth. Planet. Sci. Lett., 274, 423-438, https://doi.org/10.1016/j.epsl.2008.07.054, 2008.

Wilkes, E. B. and Pearson, A.: A general model for carbon isotopes in red-lineage phytoplankton: Interplay between unidirectional processes and fractionation by RubisCO, Geochim. Cosmochim. Acta, 265, 163-181, https://doi.org/10.1016/j.gca.2019.08.043, 2019.

Witkowski, C. R., van der Meer, M. T., Blais, B., Damsté, J. S. S., and Schouten, S.: Algal biomarkers as a proxy for pCO_2: Constraints from late quaternary sapropels in the eastern Mediterranean, Org. Geochem., 150, 104123, https://doi.org/10.1016/j.orggeochem.2020.104123, 2020.

Witkowski, C. R., Weijers, J. W., Blais, B., Schouten, S., and Damsté, J. S. S.: Molecular fossils from phytoplankton reveal secular PCO_2 trend over the Phanerozoic, Sci. Adv., 4, eaat4556, https://doi.org/10.1126/sciadv.aat4556, 2018.

Zeebe, R. E. and Wolf-Gladrow, D.: CO_2 in seawater: Equilibrium, kinetics, isotopes, Elsevier Oceanography Series, 65, Elsevier, Amsterdam2001.

Formatted: Font: (Default) Times New Roman

Zeebe, R. E., Bijma, J., and Wolf-Gladrow, D. A.: A diffusion-reaction model of carbon isotope fractionation in foraminifera, Mar. Chem., 64, 199-227, https://doi.org/10.1016/S0304-4203(98)00075-9, 1999.

Zhang, Y. G., Henderiks, J., and Liu, X.: Refining the alkenone-pCO_2 method II: Towards resolving the physiological parameter 'b', Geochim. Cosmochim. Acta, 281, 118-134, https://doi.org/10.1016/j.gca.2020.05.002, 2020.

Zhang, Y. G., Pagani, M., Liu, Z., Bohaty, S. M., and DeConto, R.: A 40-million-year history of atmospheric CO_2, Philosophical Transactions of the Royal Society A: Mathematical, Physical and Engineering Sciences, 371, 20130096, https://doi.org/10.1098/rsta.2013.0096, 2013.

Zhang, Y. G., Pearson, A., Benthien, A., Dong, L., Huybers, P., Liu, X., and Pagani, M.: Refining the alkenone-pCO_2 method I: Lessons from the Quaternary glacial cycles, Geochim. Cosmochim. Acta, 260, 177-191, https://doi.org/10.1016/j.gca.2019.06.032, 2019.

Formatted: Font: (Default) Times New Roman

Formatted: Font: (Default) Times New Roman

Formatted: Font: (Default) Times New Roman

Formatted: Font: (Default) Times New Roman

Formatted: Font: (Default) Times New Roman

Formatted: Font: (Default) Times New Roman

Formatted: Font: (Default) Times New Roman

Formatted: Font: (Default) Times New Roman